Protective Coatings for Turbine Blades
Y. Tamarin, p119-160
DOI: 10.1361/pctb2002p119

CHAPTER 7

The Effect of Protective Coatings on the Mechanical Properties of Superalloys

COATINGS PROTECT the surface of turbine blades from damage caused by high-temperature corrosion and thus preserve the structural shape of blades and their mechanical properties for the required time.

There are many papers in the technical literature that deal with experimental studies of heat resistance, fatigue strength, and thermal fatigue of coated superalloys. However, the connection between the physical and mechanical properties of protective coatings and their effect on the mechanical properties of turbine-blade superalloys has not been studied sufficiently well. For thin diffusion coatings, this can be explained by the complexity of the task, both in reproducing the correct composition and in testing the coatings separately from the alloy. However, for these coatings, information on their physical and mechanical properties is necessary for their proper application and for accurate calculations of coated-blades service lives.

The effect of coatings on mechanical properties of superalloys is a combination of several factors:

- Coating deposition alters superalloy surface stresses.
- The coating can be damaged under action of static or alternate stresses; the cracks nucleating in the coating may accelerate the superalloy damage process.
- The mechanical properties of superalloys may be affected by the coating deposition thermal cycle.
- The coating changes the surface layer microstructure of a superalloy, and this effect is boosted as high-temperature exposure time increases.

The efficiency of revealing the effect of coatings on superalloy properties depends on the testing methods employed. Cooled blades are essentially thin-walled constructions, and the effect of the coatings increases as the mismatch between the coating thickness and the blade-wall thickness rises. Thus, to correctly determine the properties of blades protected with coatings, the specimens preferable for mechanical testing should have the ratio of the coating thickness and the specimen cross section close to those of the blades in use.

Mechanical and physical properties of NiAl and Ni_3Al aluminides, which form diffusion coatings, are dealt with in numerous publications (Ref 1, 2). Such aluminide properties as ultimate strength, yield strength, and elongation values depend to a considerable extent on their structure set by the process of test-specimen fabrication and their heat treatment.

Table 7.1 refers to the test results presented in one of the earliest publications that dealt with

Table 7.1 Properties of Ni_3Al and NiAl intermetalide-base cast alloys at tensile tests at 20 °C

Aluminum content, wt%	Ultimate strength (σ_B), MPa	Yield strength ($\sigma_{0,2}$), MPa	Elongation (δ), %
13.3	205	86	1.1
14.0	280	110	1.0
25.0	163	…	0
28.0	162	…	0
30.0	103	…	0
31.5	102	…	0

Source: Ref 3

research into aluminide features (Ref 3). Mechanical properties of NiAl compound versus its test temperatures are shown in Fig. 7.1 (Ref 3, 4). Despite different elongation values for the NiAl samples reported by different authors, they agreed that, in fact, elongation-temperature relation yielded quite the same patterns. At a certain temperature dependent on a NiAl compound composition, it experiences ductile-brittle transition that is typical of all the materials with body-centered cubic lattice.

Research into the high-temperature strength of NiAl and Ni_3Al compounds has revealed that their high-temperature strength is not so high as that of superalloys. It can be improved by alloying and by forming directional or single-crystal structures (Ref 5). The previously mentioned

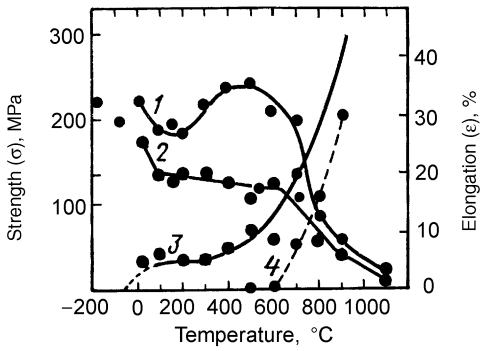

Fig. 7.1 Mechanical properties of NiAl compound of stoichiometric composition at different temperatures. 1, Ultimate strength; 2, yield strength; 3 and 4, elongation. Source: Ref 3, 4

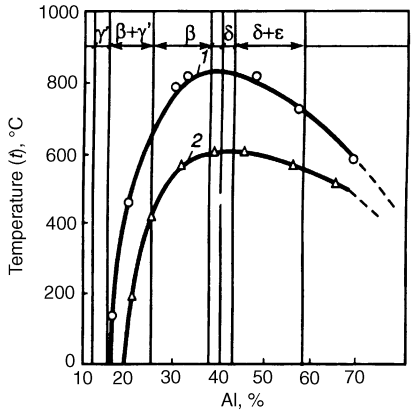

Fig. 7.2 Ductile-brittle transition temperatures for diffusion coatings ~50 μm thick with different aluminum contents of their outer layer. 1, Coatings on JS-type superalloys; 2, coatings on nickel. Source: Ref 7, 8

patterns of aluminide mechanical properties variations can be taken into consideration as a certain approximation in the research into the behavior of diffusion aluminide coatings on superalloys.

Reproducing aluminide compositions identical to numerous diffusion coating modifications is not a simple task. It is as difficult as their testing, because a sample thickness is comparable with a coating thickness. That is why the ductile-brittle transition temperature (DBTT) of a diffusion coating is recommended as its service life criterion under static and cyclic loading (Ref 6). The fact that aluminides experience ductile-brittle transition is crucial for many diffusion coatings characteristics and their effect on superalloy properties.

As an example, Fig. 7.2 demonstrates test results for diffusion coatings 50 μm thick (Ref 7, 8). The increase in aluminum content of the coatings results in the increase in their ductile-brittle transition temperature. For coatings including 16 to 17% Al, the DBTT is below 0 °C, while for coatings including 36% Al, the DBTT is ~800 °C. Ductile-brittle transition temperatures of the diffusion coatings on superalloys are higher than those of the coatings on nickel.

Thermal Expansion Coefficients and Elasticity Modulus of Coating Alloys

The mismatches between the thermal expansion coefficients (TEC) and the elasticity modulus of coatings and superalloys determine the level of stresses that arise on the blade surfaces after coating deposition, heat treatment, and under their service conditions. Thermal stresses on the surface have an effect on all the mechanical properties of coated superalloys.

For the Ni-Cr-Al and Ni-Co-Cr-Al systems, TEC studies were carried out on samples made by extruding cast billets. The Co-Ni-Cr-Al system samples are studied as-cast. To study TEC, the 0.5 to 1.0 mm thick condensates deposited by the electron beam (EB) method were also used. Before dilatometric analysis, all the samples were subjected to vacuum annealing at 1100 °C for 2 h followed by slow cooling down. The structure and phase compositions of the extruded samples are close to those of overlay coatings with the same chemical composition. Although the cast alloys feature larger structural constituent sizes, their phase composition is also

similar to that of the coatings of the same chemical composition.

Studies of TECs were carried out using a quartz dilatometer of 1500 N (made by Sincu-Rico) equipped with an induction transducer as a sensor. Sample elongation and temperature recording were carried out with the interval of 2 °C. In combination with high sensitivity of the induction transducer, it allowed detection of phase changes and transformations that cause relative variations of the sample length as small as 0.001%. The total error at measuring mean TEC was (0.25 to 0.35) · 10^{-6}, deg^{-1}, assuming confidence coefficient (P) level of $P = 0.95$. However, in the case of measuring elongation of flat samples made of condensates, the error was as high as 5 to 10%.

Dynamic modulus of elasticity was determined using the Elasomat instrument and cylindrical cast samples that were 120 mm long and 8 mm in diameter. Flat samples made of condensate with the dimensions of 100 by 10 by 2 mm were also tested. Relative errors of measuring elasticity modulus for cast samples and flat samples were 1% and 10%, respectively.

Ni-Cr-Al Alloys. The TECs for the Ni-Cr-Al system are given in Table 7.2. (Regression equations derived from statistics-based processing of the experimental data on TECs are given in the Appendix.)

Thermal expansion coefficient values for the alloy group under study are determined in each alloy by the volume ratio of its basic phase components, such as γ-solid solution, γ′-phase (Ni_3Al), β-phase (NiAl), and α-Cr. Each of these phases has TEC monotonically rising as the temperature increases, whereupon its absolute value is less for the phases with greater aluminum contents. By the mean TEC values in the temperature range of 20 to 1000 °C, the phases of the system under consideration are ranged as follows: γ (19.8 · 10^{-6}, K^{-1}), Ni_3Al (16.7 · 10^{-6}, K^{-1}), NiAl (16.3 · 10^{-6}, K^{-1}), and α-Cr (9.6 · 10^{-6}, K^{-1}).

The increase in the aluminum content of the alloy and, hence, a greater number of aluminum-rich phases (NiAl) cause reduction of the TEC mean values in the range of 20 to 1000 °C. More chromium in the alloy produces an effect similar to that of aluminum, because it leads to an α-Cr volume increase. The said general features of the effect of aluminum and chromium on the TECs of multiphase alloys of the Ni-Cr-Al system are effective up to about 600 °C; in a higher temperature range, phase transformations lead to sudden TEC variations. On consideration of the TEC effect on the coating-alloy system properties, it is not the absolute value of this characteristic that is really important but its relative value while comparing it with superalloy TECs. The Ni-Cr-Al-system alloys and superalloys are much the same in their thermal coefficients.

When overlay coatings interact with superalloys while being high-temperature tested, cobalt diffuses from the superalloys into the Ni-Cr-Al-system coatings, and after about 100 h at temperatures higher than 1000 °C, its content reaches the average cobalt content of a super-

Table 7.2 Thermal expansion coefficients, α, of Ni-Cr-Al alloys

	α · 10^6, K^{-1}									
Alloy(a)	20–100 °C	100–200 °C	200–300 °C	300–400 °C	400–500 °C	500–600 °C	600–700 °C	700–800 °C	800–900 °C	900–1000 °C
Ni14Cr3AlY	13.7	14.4	15.1	15.9	16.2	17.9	19.9	20.3	19.4	20.4
Ni18Cr5AlY	13.3	13.9	15.0	15.3	16.0	17.2	19.1	21.2	23.0	28.6
Ni20Cr6AlY	…	12.7	13.4	14.4	14.7	15.4	17.1	15.1	19.0	25.2
Ni16Cr9AlY	12.4	12.9	13.6	14.4	15.1	16.3	17.7	15.8	13.2	26.5
Ni21Cr9AlY	12.0	12.7	13.4	14.4	14.7	15.2	16.3	14.9	10.6	21.6
Ni22Cr11AlY(b)	11.7	12.6	13.2	14.6	14.8	15.5	17.2	16.9	18.7	31.0
Ni7Cr12AlY	13.1	13.7	14.4	15.4	15.7	16.9	18.6	18.6	18.6	19.7
Ni19Cr12AlY	12.0	12.7	13.4	14.0	14.8	14.3	16.1	15.0	16.2	31.1
Ni8Cr15AlY	11.8	12.6	13.5	14.0	14.3	14.6	17.6	15.3	15.6	17.0
Ni18Cr16AlY	12.2	12.8	13.3	13.8	14.6	13.2	15.1	11.3	19.3	39.1
Ni8Cr18AlY	11.6	12.6	13.4	14.4	13.7	18.4	16.1	12.0	19.7	…
Ni5Cr25Al	13.8	14.4	15.4	16.5	16.3	9.8	19.6	19.6	18.6	19.5
Ni31Al	13.4	13.9	14.3	13.0	13.3	13.9	14.4	14.5	14.6	14.8
Ni19Cr10AlY(c)	11.8	12.7	13.4	14.4	14.7	15.4	17.1	15.1	9.0	25.2
CMSX-4(d)	12.1	12.7	13.3	13.9	14.4	15.0	16.4	17.4	19.1	21.5

(a) Alloy chemical compositions are presented in Table 4.10. (b) In the range of 1000 to 1100 °C, α = 28.0 · 10^{-6}, K^{-1}; in the range of 1100 to 1200 °C, α = 22.6 · 10^{-6}, K^{-1}. (c) Condensate: nickel base, 18.5% Cr, 10.4% Al, 0.01% Y. (d) In the range of 1000 to 1100 °C, α = 25.6 · 10^{-6}, K^{-1}; in the range of 1100 to 1200 °C, α = 31.4 · 10^{-6}, K^{-1}

alloy. Therefore, when analyzing coating TEC, especially if the coatings are intended for long-term service, it is worth using the TEC values of the Ni-Co-Cr-Al system.

The results of elasticity modulus measurements for the Ni-Cr-Al alloys are given in Table 7.3. Information on statistics-based processing of experimental data is presented in the Appendix.

The value of the alloy elasticity modulus is a result of the combined elasticity modulus of the phases that form it. The NiAl (Ni8Cr18AlY)-base alloy features the lowest value of elasticity modulus, wherein, with a temperature raising to 800 °C, the modulus value does not actually change. The maximum elasticity modulus is demonstrated by the alloys whose phase composition corresponds to γ-solid solution (Ni15Cr3AlY) and γ′-phase (Ni7Cr12AlY) with the low chromium content. The value of elasticity modulus for all the alloys (except for those with the NiAl structure) monotonically decreases as the temperature rises. The absolute value of elasticity modulus for the said group of alloys is lower than that for nickel-base superalloys with an equiaxial structure.

Ni-Co-Cr-Al Alloys. To determine TECs of the Ni-Co-Cr-Al alloy major phases, these phases were extracted electrochemically and their TECs were determined by high-temperature x-ray diffraction methods. As for the Ni-Cr-Al system, their mean TEC in the temperature range of 20 to 1000 °C decreases as the aluminum content of the phases increases: γ ($17.2 \cdot 10^{-6}$, K^{-1}), Ni_3Al ($15.2 \cdot 10^{-6}$, K^{-1}), and NiAl ($13.8 \cdot 10^{-6}$, K^{-1}).

The experimental TEC data for the Ni-Co-Cr-Al-system alloys are given in Table 7.4 (Ref 9). The statistics-based processing of the experimental TEC data for the Ni-Co-Cr-Al alloys was conducted in different temperature ranges. In the temperature range of 100 to 400 °C, the influence of cobalt, chromium, and aluminum on thermal effects of TEC variations was considered. In the range of 900 to 1000 °C, the effects of TEC variations during phase transformations were discussed; in the range of 100 to 1000 °C, the effect of alloying on the mean TEC values was determined. The regression equations are given in the Appendix.

A cobalt-content increase from 10 to 30% causes an increase of the maximum TEC level for the Ni-Co-Cr-Al alloys in the temperature range of 100 to 400 °C (Fig. 7.3a). Alloying the alloys with 8 to 14% Co reduces TEC. In this case, with the chromium content raised from 15 to 30%, TEC values do not actually vary.

Aluminum, chromium, and cobalt exert a crucial effect on alloy TEC in the temperature range of 900 to 1000 °C (Fig. 7.3b). A cobalt content increase from 10 to 30% results in the reduction of the maximum TEC level. The increase in aluminum and chromium contents of the alloys causes TEC reduction too, which is mainly associated with an increase in NiAl and α-Cr volume fractions. If the aluminum, chromium, and cobalt contents of the alloys are at their maximum levels, a region with comparatively low TEC values of $\alpha < 20 \cdot 10^{-6}$, K^{-1}, appears. The TEC behavior in the temperature range of 900 to 1000 °C is well correlated with variations of the NiAl-Ni_3Al ratio, depending on alloying. The more NiAl is in the alloy, the lower the level of TEC.

The results of the research into Ni-Co-Cr-Al alloy elasticity modulus are given in Table 7.5. Due to statistics-based processing of test results, a regression equation is derived that links the

Table 7.3 Elasticity modulus, *E*, of Ni-Cr-Al alloys

	$E \cdot 10^{-2}$, MPa							
Alloy	20 °C	200 °C	300 °C	400 °C	500 °C	600 °C	700 °C	800 °C
Ni14Cr3AlY	1784	1714	1657	1601	1536	1469	1431	1354
Ni18Cr5AlY	1743	1681	1614	1564	1500	1431	1361	1304
Ni16Cr9AlY	1665	1599	1565	1510	1469	1429	1379	1348
Ni21Cr9AlY	1571	1517	1477	1438	1393	1352	1305	1270
Ni22Cr11AlY	1696	1672	1644	1612	1580	1530	1481	1441
Ni22Cr11AlY(a)	1670	…	…	…	…	…	…	1440
Ni7Cr12AlY	1806	1749	1696	1656	1609	1545	1488	1446
Ni19Cr12AlY	1596	1615	1602	1575	1545	1515	1486	1462
Ni8Cr15AlY	1424	1370	1346	1329	1315	1283	1249	…
Ni18Cr16AlY	1624	1604	1599	1579	1552	1523	1495	1469
Ni8Cr18AlY	1079	1065	1092	1091	1085	1072	1062	1047

(a) Condensate from Ni22Cr11AlY alloy

elasticity modulus value with alloying element contents of the Ni-Co-Cr-Al alloys in the temperature range of 20 to 800 °C. Calculation data available from the equations for alloy elasticity modulus at the temperatures of 20 and 800 °C are given in Fig. 7.4(a, b). Aluminum reduces the value of elasticity modulus mainly due to a higher volume of NiAl in the alloys. The cobalt effect is much stronger, especially if the aluminum content is high. The influence of both elements is explained by a rise in atom interaction energy when the nickel-base γ-solid solution is alloyed with these elements.

Elastic modulus values determined for the vapor-deposited samples are close to those determined for cast alloys (Table 7.5). These similarities are caused by measurement errors in thin, flat samples and by differences in the composi-

Table 7.4 Thermal expansion coefficients, α, of Ni-Co-Cr-Al alloys

	α · 10⁶, K⁻¹								
Alloy(a)	100–200 °C	200–300 °C	300–400 °C	400–500 °C	500–600 °C	600–700 °C	700–800 °C	800–900 °C	900–1000 °C
Ni10Co15Cr8Al	13.2	13.9	15.0	15.5	16.7	19.9	21.5	25.3	29.5
Ni30Co15Cr8Al	13.6	14.4	15.3	16.0	17.8	20.7	22.8	25.7	28.3
Ni10Co30Cr8Al	13.0	13.8	14.6	15.0	15.7	18.1	21.8	25.2	29.9
Ni30Co30Cr8Al	13.3	13.6	14.6	15.4	16.6	19.0	19.7	19.3	20.1
Ni10Co15Cr14Al	13.3	14.2	14.6	16.7	16.7	19.1	21.9	23.7	28.4
Ni30Co15Cr14Al	13.4	14.1	15.5	17.1	17.5	19.3	21.0	21.0	21.5
Ni10Co30Cr14Al	13.0	13.5	14.1	14.8	16.2	17.1	18.8	20.6	21.6
Ni30Co30Cr14Al	13.3	13.6	15.0	15.4	15.7	17.3	18.1	17.8	19.8
Ni10Co22Cr11Al	13.2	13.6	15.2	15.8	16.0	18.0	20.5	25.3	31.1
Ni30Co22Cr11Al	12.1	14.2	15.7	16.7	18.3	20.8	21.3	21.3	23.5
Ni20Co15Cr11Al	13.7	14.3	15.5	16.6	17.7	20.9	23.7	25.4	28.5
Ni20Co30Cr11Al	13.4	14.3	15.2	16.4	16.4	20.1	20.4	21.3	25.3
Ni20Co22Cr8Al	14.1	14.5	16.3	16.7	17.4	21.8	25.2	27.7	27.7
Ni20Co22Cr14Al	13.9	14.1	15.4	16.1	17.2	18.3	21.6	23.7	25.9
Ni20Co22Cr11Al	13.8	14.5	15.3	16.8	16.8	21.3	25.0	24.7	25.1
Ni20Co22Cr11AlY(b)	13.5	14.0	15.1	15.7	16.9	20.0	22.8	22.9	22.8
Ni20Co22Cr11AlY(c)	13.0	15.3	15.3	15.3	16.7	16.7	16.7	20.0	20.0
Ni6Co20Cr12AlY	13.2	13.6	15.2	15.8	16.0	18.0	20.5	25.3	31.1
Ni6Co10Cr13AlTaReHf(d)	13.2	14.2	14.7	14.2	13.6	17.5	19.2	22.1	27.8

(a) Alloys chemical compositions are presented in Table 4.11. (b) In the range of 1000 to 1100 °C, α = 25.7 · 10⁻⁶, K⁻¹; in the range of 1100 to 1200 °C, α = 23.8 · 10⁻⁶, K⁻¹. (c) Condensate from Ni20Co22Cr11AlY alloy. (d) Chemical composition: nickel base, 6.0% Co, 9.9% Cr, 12.9% Al, 3.9% Ta, 0.55% Re, 1.4% Hf, and 0.4% Si

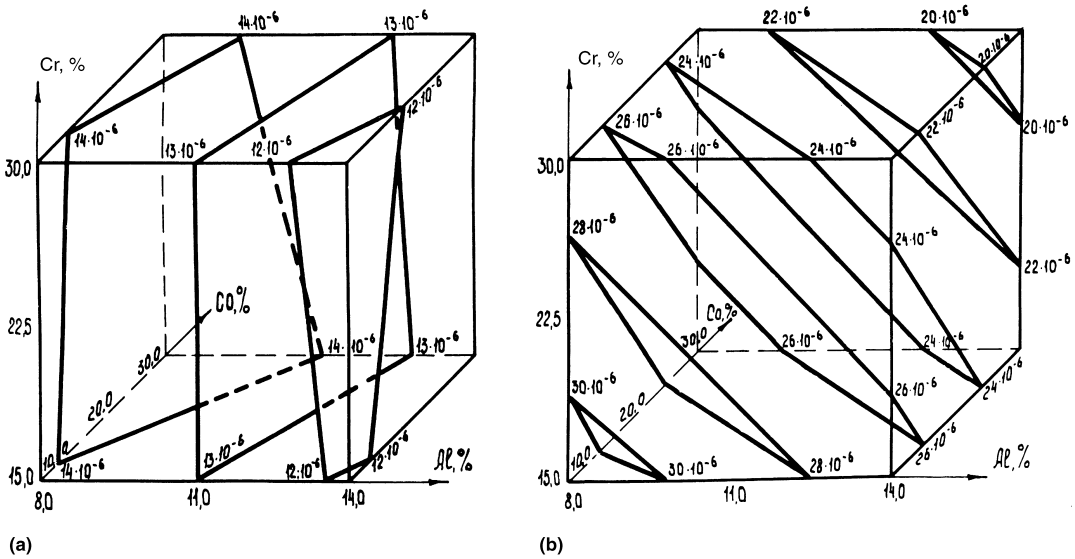

Fig. 7.3 Thermal expansion coefficients of Ni-Co-Cr-Al alloys (K⁻¹). (a) 100 to 400 °C. (b) 900 to 1000 °C

tions of the condensate samples and the alloys used for their deposition.

Co-Ni-Cr-Al Alloys. The results of the research into Co-Ni-Cr-Al-system alloy TECs are given in Table 7.6. Up to 500 °C, the temperature elevation results in a monotonical TEC rise. At the temperatures above 500 °C, an abrupt TEC change is observed due to magnetic transformation and dissolution of β- and σ-phases.

The statistics-based processing of the experimental measurement results allows for drawing the following conclusions. In the temperature range up to 500 °C, the increase in aluminum and chromium contents reduces TEC from $16 \cdot 10^{-6}$ to $13 \cdot 10^{-6}$, K^{-1}. Alloying with nickel produces the same effect. If the effect of alloying elements within the whole temperature range from 20 to 1000 °C is considered, chromium has the strongest effect on TEC. It reduces TEC. Nickel slightly reduces TEC; the effect of aluminum is not so strong.

When the temperature rises to 800 °C, the elasticity modulus of Co-Ni-Cr-Al alloys monotonically decreases to $1262 \cdot 10^2$ to $1492 \cdot 10^2$, MPa (Table 7.7). The regression equation linking elasticity modulus with alloying element content and temperature is given in the Appendix. The effect of the alloying elements is similar at both low and high temperatures.

Mechanical Properties of Coating Alloys

The coatings deposited on turbine blade surfaces are affected by the same static and alternate stresses that have an impact on the blade materials. The level of coating mechanical properties has an effect on the basic characteristics of blades, such as their high-temperature strength, endurance, and thermal fatigue. Determining the mechanical properties is a hard task. Even fabrication of cast samples of the alloys with high aluminum content is hampered by their low ductility. It is also worth taking into account that at high-temperature testing and using the blade coatings, their compositions and properties vary continuously.

Strength and ductility of the alloys used for coatings were investigated using the standard procedures for cast and vapor-deposited samples. The cast samples 5 mm in diameter and the flat samples 0.5 to 1.0 mm thick made by vapor deposition were annealed before testing at 1050 °C for 4 h.

Test results for Ni-Cr-Al-system alloys are presented in Tables 7.8 and 7.9 and in Fig. 7.5. The Ni20Cr6AlY alloy with $(\gamma + \gamma')$-phase composition features moderate-strength values. Ductility of this alloy at temperatures up to 1000 °C does not exceed 5%. The Ni8Cr15AlY alloy based on Ni_3Al has higher strength. At temperatures above 800 °C, its strength exceeds the strength of all the alloys studied. Ductility of the alloys with $(\gamma + \gamma')$-phase composition depends on the aluminum content and other alloying elements. The Ni_3Al-base systems are used for fabrication of superalloys and can be considered most promising for designing the coatings highly resistant to thermal fatigue.

The Ni22Cr11AlY alloy is most widely used as a coating on blades operating under conditions of high temperatures and thermal stresses.

Table 7.5 Elasticity modulus, *E*, of Ni-Co-Cr-Al alloys

	$E \cdot 10^{-2}$, MPa							
Alloy	20 °C	200 °C	300 °C	400 °C	500 °C	600 °C	700 °C	800 °C
Ni10Co15Cr8Al	1560	1499	1461	1461	1394	1358	1300	1237
Ni30Co15Cr8Al	1699	1637	1586	1533	1482	1439	1357	1267
Ni10Co30Cr8Al	1664	1602	1573	1538	1491	1449	1404	1322
Ni30Co30Cr8Al	1858	1799	1747	1705	1662	1661	1556	1473
Ni10Co15Cr14Al	1307	1308	1301	1286	1274	1255	1233	1173
Ni30Co15Cr14Al	1550	1523	1501	1476	1446	1414	1373	1316
Ni10Co30Cr14Al	1364	1341	1324	1306	1278	1259	1238	1193
Ni10Co22Cr11Al	1486	1461	1440	1404	1373	1337	1299	1249
Ni30Co22Cr11Al	1737	1688	1656	1625	1583	1541	1496	1426
Ni20Co15Cr11Al	1566	1530	1500	1472	1435	1400	1359	1302
Ni20Co22Cr8Al	1602	1548	1506	1472	1431	1379	1318	1263
Ni20Co22Cr11Al	1633	1595	1563	1533	1496	1464	1422	1373
Ni20Co22Cr11AlY(a)	1549	1514	1476	1444	1410	1365	1311	1248

(a) Condensate from Ni20Co22Cr11AlY alloy

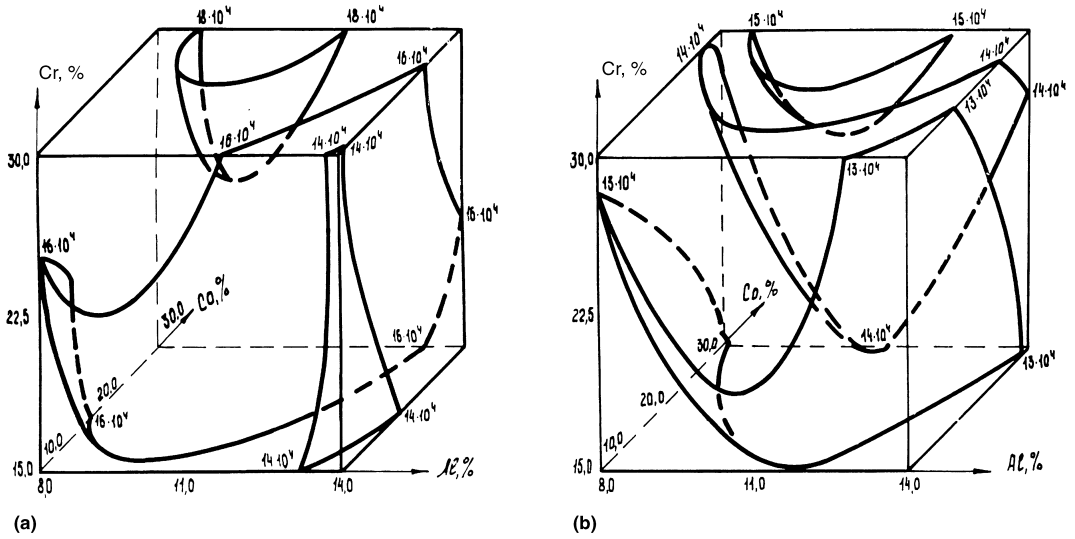

Fig. 7.4 Elasticity modulus of Ni-Co-Cr-Al alloys (MPa). (a) 20 °C. (b) 800 °C

Table 7.6 Thermal expansion coefficients, α, of Co-Ni-Cr-Al alloys

	$\alpha \cdot 10^6$, K^{-1}									
Alloy(a)	20–100 °C	100–200 °C	200–300 °C	300–400 °C	400–500 °C	500–600 °C	600–700 °C	700–800 °C	800–900 °C	900–1000 °C
Co10Ni15Cr6AlY	14.3	15.2	16.1	17.1	17.8	21.4	35.5	23.1	20.2	20.5
Co30Ni15Cr6AlY	12.8	13.6	14.6	15.5	16.5	17.3	18.0	19.0	20.3	22.0
Co10Ni30Cr6AlY	13.7	14.2	14.9	15.5	16.2	19.2	20.6	19.2	18.7	18.2
Co30Ni30Cr6AlY	13.3	14.2	15.1	16.1	16.7	19.3	21.7	25.2	18.1	15.6
Co10Ni15Cr12AlY	13.9	14.9	15.7	16.9	17.5	19.9	27.6	27.7	21.3	15.4
Co30Ni15Cr12AlY	13.8	14.7	15.7	16.7	17.4	18.8	20.3	21.4	20.3	20.3
Co10Ni30Cr12AlY	12.3	12.9	13.5	14.2	14.8	15.3	15.8	16.5	19.2	21.7
Co10Ni22Cr9AlY	13.8	14.3	14.8	15.3	16.6	17.6	15.6	14.8	16.8	21.8
Co30Ni22Cr9AlY	13.4	14.0	14.7	15.7	16.2	17.5	22.5	22.8	20.1	…
Co20Ni15Cr9AlY	14.2	14.9	15.6	16.5	17.1	19.4	26.6	21.0	18.9	18.5
Co20Ni30Cr9AlY	12.8	13.5	14.0	14.8	15.8	17.0	18.8	15.6	…	…
Co20Ni22Cr6AlY	13.8	14.6	15.3	16.1	16.8	19.3	22.4	19.3	16.8	18.1
Co20Ni22Cr12AlY	13.0	13.6	14.5	15.3	16.5	17.4	19.0	17.3	18.5	23.3
Co20Ni22Cr9AlY	13.1	13.8	14.4	15.2	16.1	18.0	19.9	18.6	17.0	20.6
Co22Cr9AlY	…	13.3	13.7	14.1	14.5	14.8	14.8	14.7	15.2	16.1

(a) Alloy chemical compositions are presented in Table 4.13

Table 7.7 Elasticity modulus, *E*, of Co-Ni-Cr-Al alloys

	$E \cdot 10^{-2}$, MPa								
Alloy	20 °C	100 °C	200 °C	300 °C	400 °C	500 °C	600 °C	700 °C	800 °C
Co10Ni15Cr6AlY	2071	1956	1874	1809	1738	1662	1573	1492	1262
Co30Ni15Cr6AlY	1893	1856	1803	1740	1655	1601	1549	1386	1266
Co10Ni30Cr6AlY	1960	1923	1861	1792	1702	1618	1535	1447	1353
Co30Ni30Cr6AlY	1820	1787	1726	1683	1603	1549	1469	1366	1284
Co10Ni15Cr12AlY	1956	1911	1839	1779	1703	1641	1568	1458	1334
Co30Ni15Cr12AlY	1826	1787	1763	1714	1674	1621	1554	1463	1308
Co10Ni22Cr9AlY	2013	1982	1937	1888	1823	1764	1690	1625	1492
Co30Ni22Cr9AlY	1820	1795	1749	1704	1649	1575	1516	1434	1345
Co20Ni15Cr9AlY	1792	1759	1706	1657	1586	1540	1666	1363	1295
Co20Ni30Cr9AlY	2037	2006	1970	1919	1866	1805	1739	1679	1492
Co20Ni22Cr6AlY	1888	1843	1781	1717	1648	1576	1476	1372	1289
Co20Ni22Cr12AlY	1778	1760	1728	1702	1662	1643	1578	1515	1438
Co20Ni22Cr9AlY	1847	1799	1749	1700	1646	1600	1534	1426	1344

Its properties are typical of all the materials of the Ni(Co)-Cr-Al system used for depositing overlay coatings. At temperatures under 800 °C, the alloy features high strength, which abruptly diminishes as the temperature rises to 1100 °C. At 500 °C, elongation of the Ni22Cr11AlY alloy does not exceed 3%. However, at higher temperatures, elongation increases abruptly to 69% at 1100 °C. Such a change in the properties of this alloy is due to the development of phase transformations. Intensive softening of the Ni20Cr12AlY alloy starts at temperatures above 700 °C, when γ'-phase is dissolving in the alloy.

Tables 7.10 and 7.11 and Fig. 7.5 present the test results on the mechanical properties of the Ni-Co-Cr-Al alloys. At temperatures below 600 °C,

Table 7.8 Ultimate strength, σ_B, of Ni-Cr-Al alloys

	σ_B, MPa							
Alloy	**500 °C**	**600 °C**	**700 °C**	**800 °C**	**900 °C**	**975 °C**	**1000 °C**	**1100 °C**
Ni22Cr11AlY	728	…	672	396	216	…	68	34
Ni22Cr6AlY	316	…	406	341	306	…	236	…
Ni20Cr6AlY(a)	550	530	390	190	…	…	65	…
Ni8Cr15AlY(a)	…	650	500	…	400	358	…	157
Ni5Cr25Al	…	300	250	…	200	150	120	50

(a) Samples are vapor deposited from alloy of the said composition

Table 7.9 Elongation, δ, of Ni-Cr-Al alloys

	δ, %								
Alloy	**500 °C**	**600 °C**	**700 °C**	**800 °C**	**900 °C**	**975 °C**	**1000 °C**	**1100 °C**	**1200 °C**
Ni22Cr11AlY	…	…	24	31	74	…	105	…	…
Ni22Cr6AlY	1	…	1.2	2.4	2.6	…	3.2	…	…
Ni20Cr6AlY(a)	16	…	16	…	49	…	85	…	…
Ni8Cr15AlY(a)	…	0	0	…	10	12	…	31	…
Ni5Cr25Al	…	0	10	…	20	25	30	…	70

(a) Samples are vapor deposited from alloy of said composition

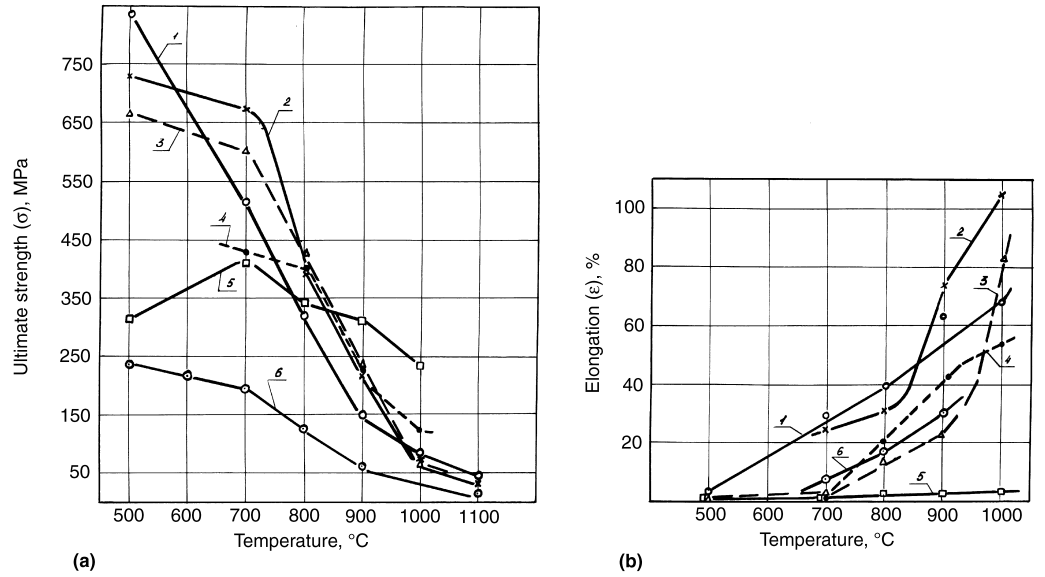

Fig. 7.5 (a) Ultimate strength and (b) elongation of alloys. 1, Ni20Co20Cr12AlY; 2, Ni20Cr12AlY; 3, Ni10Co20Cr12AlY; 4, Co20Cr12AlY; 5, Ni20Cr7AlY; 6, NiAl (33% Al)

the Ni20Co20Cr12AlY and Ni10Co20Cr12AlY alloys have high ultimate strength and relatively low ductility ($\delta < 5\%$). As the temperature rises, the alloy strength diminishes monotonically, and at 1100 °C, it is 30 to 40 MPa. Ductility of the alloys under study rises monotonically, and at temperatures above 1000 °C, some alloys (e.g., Ni10Co22Cr11AlY) are in a superductile state; their elongation exceeds 100%. Different alloy behaviors, which manifest themselves in temperature-dependent variations of their strength and ductility parameters, are caused by their phase composition and alloying with cobalt. In the temperature range higher than 600 °C, the Ni20Co20Cr12AlY alloy alloyed with 20% Co shows no trace of γ'-strengthening phase. It has $(\beta + \gamma)$ phase composition, which causes an abrupt drop of its ultimate strength and an increase of its ductility as the temperature rises.

Cobalt-base alloys also feature monotonically decreasing strength and increasing ductility as the temperature rises from 500 to 1100 °C (Tables 7.12 and 7.13 and Fig. 7.5). The strength of these alloys depends slightly on their alloying. It is related to the fact that the said system lacks γ'-strengthening phase. The Appendix contains the regression equations linking strength and ductility of the Co-Ni-Cr-Al-Y-system alloys with their alloying element contents.

The comparison of strength and ductility of the cast and vapor-deposited samples of the

Table 7.10 Yield strength ($\sigma_{0,2}$) and ultimate strength (σ_B) of Ni-Co-Cr-Al alloys

	$\sigma_{0,2}$, MPa			σ_B, MPa					
Alloy	800 °C	900 °C	1000 °C	500 °C	700 °C	800 °C	900 °C	1000 °C	1100 °C
Ni10Co15Cr8AlY	…	335	178	…	…	698	415	219	70
Ni30Co15Cr8AlY	…	246	103	…	…	572	268	112	41
Ni10Co30Cr8AlY	343	194	73	…	…	434	234	88	56
Ni10Co22Cr11AlY	…	…	…	668	602	429	233	62	…
Ni10Co20Cr12AlY(a)	…	…	…	…	…	260	190	55	…
Ni20Co22Cr8AlY	344	230	72	…	…	470	249	82	48
Ni20Co22Cr11AlY	292	113	69	840	514	319	148	84	45
Ni20Co20Cr12AlY(a)	…	…	…	520	510	320	…	50	…

(a) Samples are vapor deposited from alloy of the said composition.

Table 7.11 Elongation (δ) of Ni-Co-Cr-Al alloys

	δ, %					
Alloy	500 °C	700 °C	800 °C	900 °C	1000 °C	1100 °C
Ni10Co15Cr8AlY	…	…	4	7	14	34
Ni30Co15Cr8AlY	…	…	5	7	15	37
Ni10Co30Cr8AlY	…	…	27	32	68	66
Ni10Co22Cr11AlY	0.5	3	14	23	84	…
Ni10Co20Cr12AlY (a)	…	…	…	3	130	…
Ni20Co22Cr8AlY	…	…	20	41	42	15
Ni20Co22Cr11AlY	4	28	39	65	68	…
Ni20Co20Cr12AlY (a)	3	…	25	70	130	…

Condensate from alloy of said composition

Table 7.12 Yield strength ($\sigma_{0,2}$) and ultimate strength (σ_B) of Co-Ni-Cr-Al alloys

	$\sigma_{0,2}$, MPa			σ_B, MPa			
Alloy	500 °C	700 °C	900 °C	500 °C	700 °C	900 °C	1100 °C
Co10Ni22Cr9AlY	496	392	161	567	546	205	60
Co30Ni22Cr9AlY	…	428	126	…	547	165	57
Co20Ni15Cr9AlY	392	315	122	690	461	142	42
Co20Ni30Cr9AlY	564	479	165	866	567	173	54
Co20Ni22Cr6AlY	494	334	158	787	496	190	53
Co20Ni22Cr12AlY	…	202	…	…	474	249	64
Co20Ni22Cr9AlY	493	376	178	810	531	188	60

Ni20Co20Cr12AlY alloy (Fig. 7.6a,b) demonstrates that the principal trend of properties change versus temperature is the same. At the same time, the mechanical properties of the vapor-deposited sample are slightly worse than those of the cast sample (50 and 84 MPa at 1000 °C, respectively), but its ductility is higher. The vapor-deposited and cast samples of other alloys have the same relationship between their properties. Differences in the properties are explained by structural differences, such as more dispersed phases in the vapor-deposited samples, different chemical compositions of vapor-deposited samples and evaporated alloys, and sample shapes and sizes.

To determine the moment when the alloys become ductile, the alloys of the Ni-Cr-Al and Ni-Co-Cr-Al systems were bend tested. Testing was carried out by applying certain steady loading to the central part of the sample and then measuring its strain. The test samples were fabricated by the extrusion method and had a dispersed structure similar to that of vapor-deposited samples and coatings.

The Ni20Co20Cr12AlY alloy experiences deformation even at room temperature. At 500 °C, the sample is quite ductile when bent (Fig. 7.7). The cobalt-free alloy of the same chromium and aluminum contents demonstrates noticeable strains only at 600 °C. The Ni10Co15Cr8AlY and Ni30Co15Cr8AlY alloys differing only in cobalt contents have different ductility levels. The 30% Co alloy becomes ductile even at room temperature, while the 10% Co alloy becomes ductile at temperatures above 500 °C. The increase in aluminum content of the alloy up to 14% results in overriding the cobalt effect. The high aluminum content and, respectively, high NiAl content (of 70 to 80%) raise the alloy plasticization temperature to 800 °C.

The previously mentioned test results show that at 500 to 1000 °C, the strength levels of the cast alloys used for coatings, their vapor-deposited samples, and the respective coatings are considerably lower than those of modern superalloys. That is why the protective coating cannot bear any static and alternate stresses generated in turbine blades. This should be taken into account when calculating stresses and strains in coated turbine blades.

Table 7.13 Elongation, δ, of Co-Ni-Cr-Al alloys

	δ, %			
Alloy	**500 °C**	**700 °C**	**900 °C**	**1100 °C**
Co10Ni22Cr9AlY	1	13	49	74
Co30Ni22Cr9AlY	…	15	27	37
Co20Ni15Cr9AlY	11	19	72	61
Co20Ni30Cr9AlY	12	29	66	72
Co20Ni22Cr6AlY	9	25	53	56
Co20Ni22Cr12AlY	…	…	37	57
Co20Ni22Cr9AlY	10	28	50	63

Thermal Stresses in Superalloy Coatings

A study of the coating stressed state is one of the basic elements used for development of coatings and their use. Thermal stress generation during heating and cooling of coated parts caused by a mismatch between the TECs of a coating and a superalloy is typical for both diffusion and overlay coatings.

Thermal stress in a coating (σ_c) may be calculated from a ratio of coating and superalloy TECs:

$$\sigma_c = E_c \cdot \frac{(\alpha_c - \alpha_{sa}) \cdot (T - T_0)}{1 - \mu_c}$$

where E_c is coating modulus of elasticity; α_c and α_{sa} are TECs of a coating and a superalloy in the temperature range of T_0 to T, respectively; T_0 is a temperature of zero thermal stress level in a coating-superalloy system; T is a current temperature; and μ_c is Poisson's ratio of a coating.

Thermal stresses generated in the coating-superalloy system are crucial to the destruction of the coating on turbine blade surfaces during heating and cooling under transient conditions typical of aircraft gas-turbine engines.

Experimental Studies of Thermal Stresses. To study stressed coatings, two methods were used:

- Technique for measurement of strain caused by coating chemical removal from a sample surface
- X-ray diffraction technique for assessing coating stresses by measuring crystal lattice strain (Ref 10, 11)

As mentioned in many publications, compressive stresses occur in diffusion aluminide coatings at room temperature. Their generation is caused by two factors:

- When nickel superalloys undergo aluminizing, $NiAl_3$, Ni_2Al_3, NiAl, and Ni_3Al form, their specific volumes (0.25, 0.21, 0.17, and

0.14 cm^3/g, respectively) being larger than the specific volume of the superalloy (0.11 to 0.12 cm^3/g).

- Thermal expansion coefficients of aluminides are less than those of superalloys.

The compressive stress level in aluminide coatings depends on the aluminizing technique in use. The results of the studies pursued show that on aluminizing a nickel superalloy of JS-type from the slurry containing 100% Al at the temperature of 700 °C for 4 h, the residual compressive stress of $\sigma = -200$ MPa generates in the coating surface layer at room temperature. In the coating applied by aluminizing at 950 and 1200 °C for 4 h, the compressive stresses are −160 and −140 MPa, respectively.

The stress level in diffusion coatings decreases with the temperature increase. The data on thermal stresses in the diffusion coating measured by the x-ray method at elevated temperatures are presented in Fig. 7.8. The coating was applied by aluminizing the JS6U superalloy in a

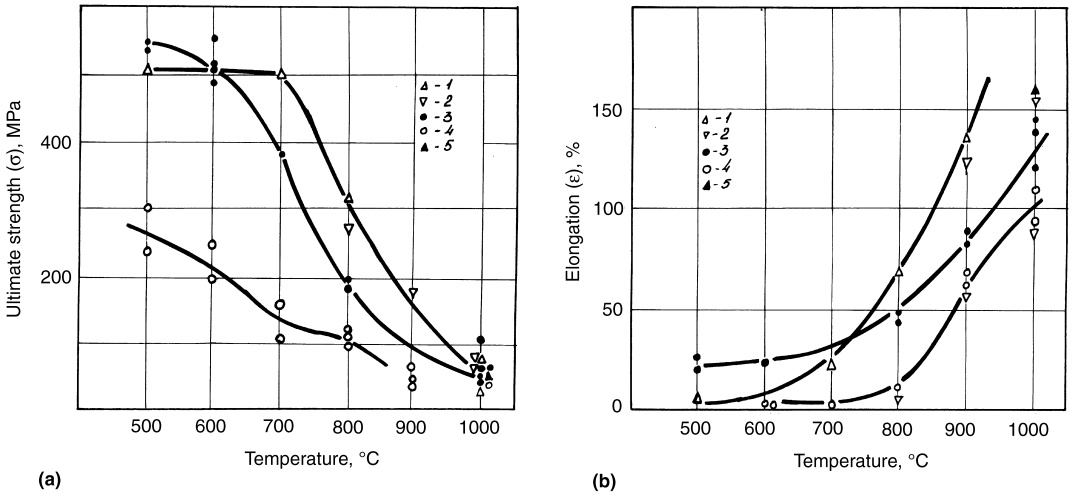

Fig. 7.6 (a) Ultimate strength and (b) elongation of samples made from alloy condensates. 1, Ni20Co20Cr12AlY; 2, Ni10Co20Cr12AlY; 3, Ni20Cr7AlY; 4, Ni5Cr8AlY; 5, Ni20Cr12AlY

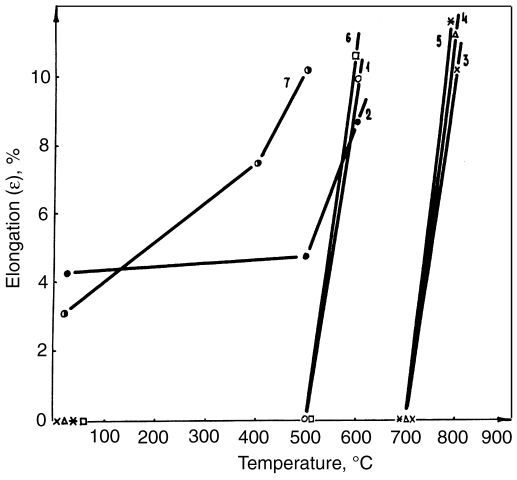

Fig. 7.7 Ductility of alloys during bend testing. 1, Ni10Co15Cr8Al; 2, Ni30Co15Cr8Al; 3, Ni10Co30Cr8Al; 4, Ni10Co15Cr14Al; 5, Ni30Co15Cr14Al; 6, Ni22Cr11AlY; 7, Ni20Co22Cr11AlY

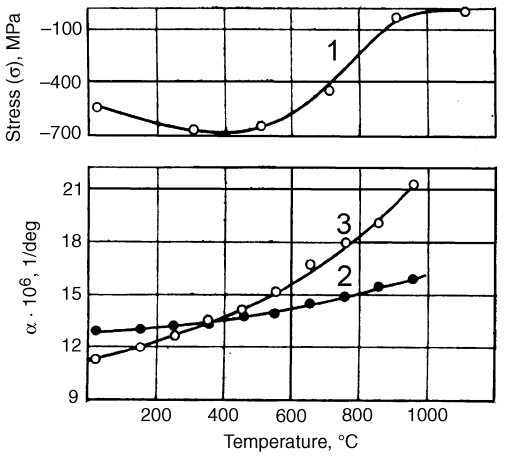

Fig. 7.8 Thermal stresses in (1) diffusion coating on JS6U superalloy versus temperature. Thermal expansion coefficients of (2) NiAl and (3) superalloy. Source: A.I. Samoilov and I.A. Ignatova

mixture of 98% Al-Fe alloy (50% Al) and 2% NH_4Cl at 950 °C for 4 h. The extreme points on the stress-temperature curve are caused by different TECs of the superalloy and the coating-base aluminide. At high-temperature testing, the stress level of the diffusion coating depends on its test time and temperature. However, on cooling from the test temperature, the compressive stresses always rise in diffusion coatings.

When analyzing a stressed state of an overlay coating, it is necessary to take into account the following initial conditions. When the EB method is used, the coating is deposited on a substrate heated to 850 to 950 °C, and evaporation heat generated during its condensation also heats its thin surface layers. Despite the fact that no special preheating equipment is used at electric arc (EA) deposition, the substrate is heated by plasma flow up to 500 to 600 °C. Under these conditions, no stresses are generated at the interface of the coating and the substrate on which the coating is deposited from vapor or plasma.

At the heat treatment temperatures of 1000 to 1050 °C, the coatings are in a ductile or, in some cases, superductile state ($\delta > 100\%$); their yield stress is lower than 50 MPa. In addition, at ~1000 °C, recrystallization occurs in the coatings of the Ni-Cr-Al and Ni-Co-Cr-Al systems. On cooling from ~1000 °C, a mismatch between the TECs of the coating and the protected alloy causes thermal stress generation. As the temperature decreases, thermal stresses increase and reach their maximum at room temperature.

The results of x-ray diffraction analysis of stresses at different stages of the coating deposition process and their heat treatment and machining are shown in Fig. 7.9. The coatings 80 to 100 μm thick made of Ni20Cr12AlY, and Ni20Co20Cr12AlY alloys were deposited by the EB method. All the measurements were carried out at room temperatures; the JS6U superalloy was used as a substrate material.

The tensile stress level of +(70 to 90) MPa is typical of the coatings as-deposited by the EB method on the substrate heated to 850 to 950 °C. On annealing at 1030 °C for 2 h, tensile stresses in the coatings increase. The tensile stress level in the coating alloyed with cobalt is higher. On annealing at 1030 °C of the Ni20Cr12AlY coating applied by the EA method, its tensile stress level is +90 MPa. This indicates that the level of tensile stresses in the coatings depends little on a deposition technique and is mainly determined by a mismatch between the TECs of the coating and the superalloy.

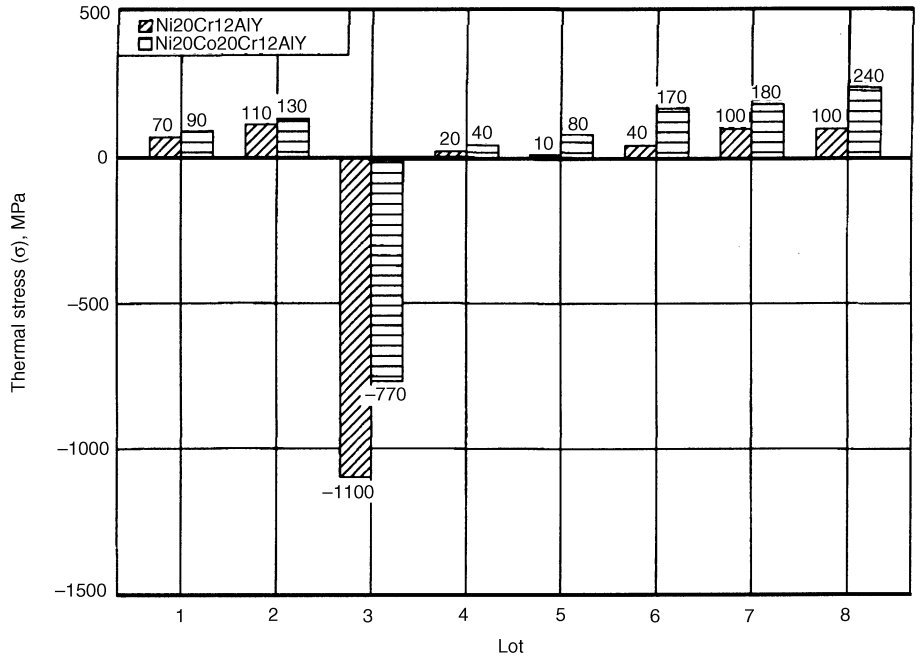

Fig. 7.9 Thermal stresses at 20 °C in overlay coatings on JS6U superalloy after different technological treatment processes. 1, after deposition (D); 2, after D + annealing; 1030 °C, 2 h (A); 3, after (D + A) + peening (P); 4, after (D + A + P) + annealing: 700 °C, 2 h; 5, after (D + A + P) + annealing: 800 °C, 2 h; 6, after (D + A + P) + annealing: 900 °C, 2 h; 7, after (D + A + P) + annealing: 1000 °C, 2 h; 8, after (D + A + P) + annealing: 1030 °C, 2 h

The next step in the technological process for the coatings deposited by the EB method is a compacting treatment by microball peening, which generates high compressive stresses, whereupon their absolute value exceeds that for the Ni20Cr12AlY coating. This is due to a higher yield stress of this coating at room temperature.

Annealing the specimens peened with microballs at a temperature above 700 °C completely eliminates coating strain hardening. On annealing of the specimen peened with microballs, all stresses are relaxed and tensile stresses regenerate during cooling. The threshold recrystallization temperature for the Ni20Cr12AlY coating is ~1000 °C.

The processes of stress relaxation in the coating alloyed with cobalt run in another manner, compared with the Ni20Cr12AlY coating. This is because coating strain hardening and its subsequent heat treatment initiate phase transformations and recrystallization. This results in a steadier state, compared to as-deposited and as-annealed for the first-time coating. The increase in thermal stresses of the Ni20Co20Cr12AlY coating is caused by a greater mismatch between its TEC and that of the JS6U superalloy, compared with the Ni20Cr12AlY coating and the JS6U superalloy.

The stressed Ni20Cr12AlY and Ni20Co20Cr12AlY coatings were x-rayed in the temperature range from room temperature to 900 °C. The specimens tested were subjected to a full treatment cycle, including annealing at 1030 °C for 2 h, microball peening, and final annealing at 1030 °C for 2 h. The results of the investigation are shown in Fig. 7.10. Stresses were gradually relaxing in both coatings. For the Ni20Cr12AlY coating, the coating-alloy system shows no stresses at 800 °C. Further temperature increases to 900 °C result in the generation of low compressive stresses (~20 MPa). When cooling the alloy from the said temperature to room temperature, stresses recover to their previous level.

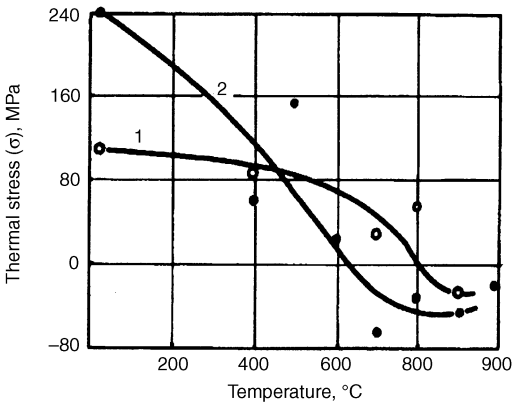

Fig. 7.10 Thermal stresses in (1) Ni20Cr12AlY coating and (2) Ni20Co20Cr12AlY coating on JS6U superalloy

In the Ni20Co20Cr12AlY coating, the temperature increase results first in the abrupt drop of tensile stresses from 240 MPa at 20 °C to 0 MPa at 650 °C, then in the generation of low compressive stresses (−50 MPa); as the temperature approaches 900 °C, their absolute value decreases to −20 MPa. The compressive stress generation in the Ni20Cr12AlY and Ni20Co20Cr12AlY coatings is explained once again by a mismatch between the TECs of the coating and the alloy.

The results of the research into thermal stresses using the technique of strain measuring during chemical removal of coatings are shown in Fig. 7.11. The stresses were measured in samples cut out of blades made of the JS6U superalloy and subjected to annealing at 1030 °C for 2 h, compacting by microball peening, and further annealing at 1030 °C for 2 h. Tensile stresses at a distance of 20 μm from the surface of the Ni20Cr12AlY coating are 100 to 180 MPa. With due account of possible errors introduced by both methods, these results are in good agreement with the results of x-ray diffraction. As the distance from the surface increases, the stresses gradually decrease, and at a distance equal to the coating thickness, the stresses approximate to a zero level. The study of the stressed coating on the blades subjected to testing in an engine for ~100 h demonstrates that both the sign and the level of the stresses do not actually change.

The experimental methods allow assessment of the stressed state of the coated specimen surfaces. However, these methods are rather time-consuming and may introduce considerable errors when the changes in chemical and phase compositions take place during high-temperature testing. The method based on etching off coatings allows studying the stressed state only at their room temperature.

The use of calculation methods allows the analysis of the coating physical and mechanical properties effect on their thermal stress levels, as well as the assessment of design features of any type and composition of multilayer coatings deposited on substrates of any type. The calcu-

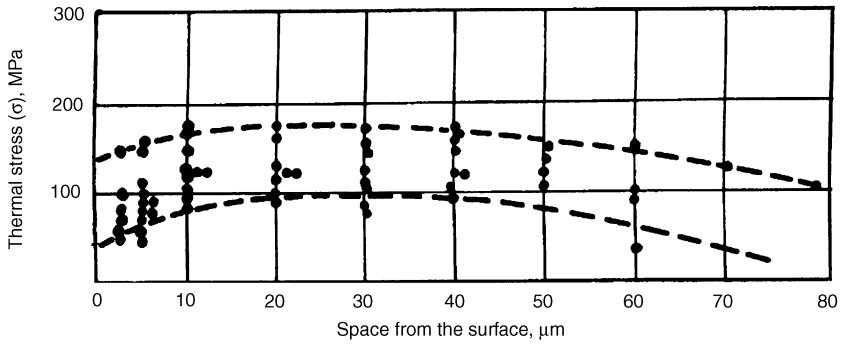

Fig. 7.11 Distribution of thermal stresses at 20 °C in Ni20Cr12AlY coating on JS6U superalloy blades

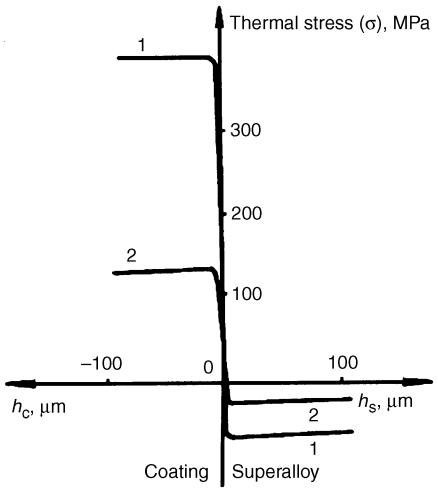

Fig. 7.12 Calculated thermal stresses at 20 °C in (1) Ni20Co20Cr12AlY coating and (2) Ni20Cr12AlY coating on JS6U superalloy specimens. h_c, distance from a "coating alloy" interface into the coating; h_s, distance into the alloy

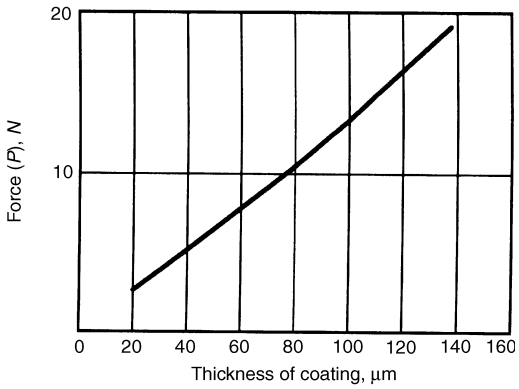

Fig. 7.13 Forces (*P*) acting in Ni22Cr12AlY coating on JS6U superalloy versus coating thickness

lation methods are a step toward controlling stresses in coatings and the respective characteristics of their thermal fatigue.

Coating-Thermal-Stresses Modeling. To calculate the thermal stresses occurring in the coating-superalloy system, a strained body stressed-state numerical modeling method was used (Ref 12). The specimen taken for model calculation was 2 mm thick and 4 mm long; a coating 0.1 mm thick was applied to one of its sides. The length of 4 mm allows elimination of any edge effect.

On the basis of the previously mentioned x-ray diffraction results, within tolerable limits, the T_0 temperature was taken to be 920 °C. At the T_0 temperature, the stresses at the coating/superalloy interface approximate to a zero level. Thermal expansion coefficients and modulus of elasticity determined from the investigation of the coating alloys were used for calculations.

The calculation results for the stresses occurring in the Ni20Cr12AlY coating/JS6U superalloy and the Ni20Co20Cr12AlY coating/JS6U superalloy systems at their cooling from 920 to 20 °C are shown in Fig. 7.12. The calculated stresses in the surface layer of the Ni20Co20Cr12AlY coating are +392 MPa, while in the surface layer of the Ni20Cr12AlY coating they are +128 MPa. The coated specimen surface stress profile shows that the tensile stresses peak is in the coating zone near the coating/alloy interface. In the vicinity of the interface, the stress sign reverses abruptly, and compressive stresses are observed in the alloy. Beneath the Ni20Co20Cr12AlY coating, compressive stresses reach −8 MPa; beneath the Ni20Cr12AlY coating they are −2 MPa. The compressive stresses gradually decrease as the

distance from the coating/alloy interface increases.

The diagram showing the value of forces in the coating-alloy system versus coating thickness is presented in Fig. 7.13. The force, P, in the coating was calculated from the following formula:

$$P_n = \sum_{i=1}^{n} \cdot \sigma_i \cdot F_i$$

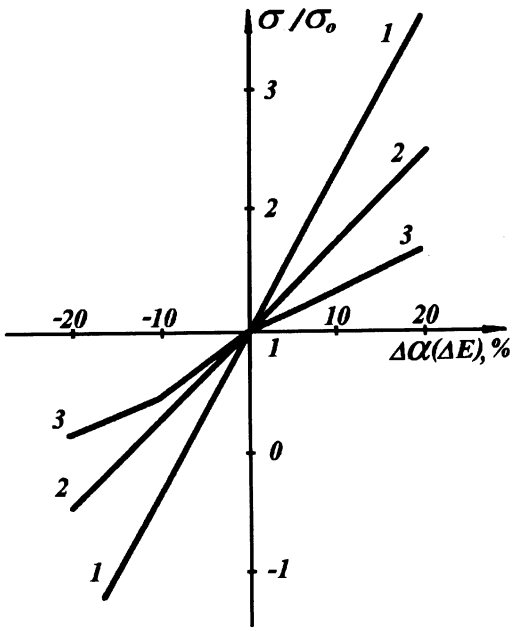

Fig. 7.14 Level of thermal stress ratio, σ/σ_0, in (1, 3) coating and in (2) substrate versus (1, 2) coating thermal expansion coefficient variation, $\Delta\alpha$, and (3) superalloy elasticity modulus, ΔE

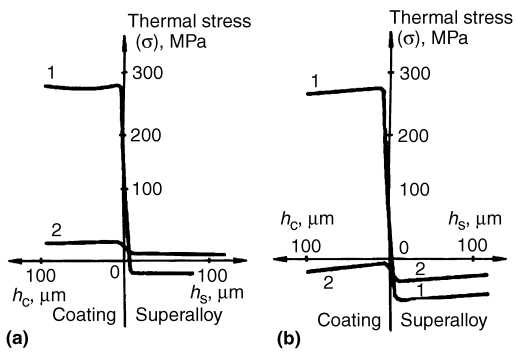

Fig. 7.15 Calculated thermal stresses in (1) Ni20Co20Cr12AlY and (2) Ni20Cr12AlY coatings on JS6F superalloy specimens. Orientations of (a) [001] and (b) [111]

where σ_i is stress in the sections into which the coating is divided; F_i is the area affected by stress σ_i; and n is the number of sections into which the coating is divided.

The separation of the stresses and forces acting in the coating has a physical meaning. The stresses in the coating have an effect on the coating material and may cause its failure. The forces in the coating are applied to the coating/alloy interface and may cause spalling of the coating along this interface. The force in the coating increases monotonically as the coating becomes thicker. Thus, coating thickness is limited by the strength of the coating/coated alloy interface (i.e., by its adhesive strength). The unsatisfactory adhesive strength level may cause spontaneous spallation of a "thick" coating. Spalling from the substrate surface may occur without any stress applied.

Superalloy TECs vary slightly, depending on their alloying. Coating TECs can vary within a rather wide range. Coating TECs also vary during high-temperature testing due to the change of the coating chemical and phase compositions.

The calculated thermal stresses in the coating and the substrate versus differences of TEC ($\Delta\alpha$) and elasticity modulus (ΔE) for the coating and superalloy are shown in Fig. 7.14. The Ni20Cr12AlY coating/JS6U superalloy system was taken as the basis for calculation. Coating and substrate stresses vary linearly with $\Delta\alpha$. As a TEC mismatch between the coating and alloy increases by 20%, the level of thermal stresses in the coating increases 3.7 times. The $\Delta\alpha$ has a weaker effect on the stresses in the substrate. The effect of ΔE on the stresses in the coating is not strong.

The calculation results for thermal stresses in single-crystal specimens made of JS6F superalloy with grain orientations of [001] and [111] are given in Fig. 7.15. The Ni20Cr12AlY and Ni20Co20Cr12AlY coatings are deposited on the specimens. In the case of the Ni20Cr12AlY coating, the stress level in the substrate with the orientation of [001] is $+29$ MPa, while in the case of the Ni20Co20Cr12AlY coating it is $+275$ MPa. The stress level in the coatings on the specimens with the orientation of [111] is lower.

The main factor, which decides the value of thermal stresses, is a mismatch between the coating and alloy TECs. If this mismatch is not great, as for the Ni20Cr12AlY coating, the variation of elasticity modulus is crucial to the value and sign of thermal stresses. If the mismatch is high,

the use of the material with a high elasticity modulus has a minor effect on the thermal stress level, which decreased by only 5% for the Ni20Co20Cr12AlY coating.

The development of multilayer coating systems is very promising and can improve coating stability, for example, in the case of applying the Ni_3Al layer or thermodynamically stable carbides (NbC, HfC) to the coating/alloy interface. By using multilayer coatings, it is possible to control the level of thermal stresses in them. The experimental determination of stresses in multilayer systems is a complicated process and, as a rule, it is reduced to measuring total stresses. The results of thermal stress calculations for different modifications of two-layer coatings are shown in Fig. 7.16. Depending on the position in the coating pattern, the layers of the same chemical composition may have different stress signs.

Effect of Coatings on High-Temperature Strength of Superalloys

High-temperature strength of the protective coating materials is substantially lower than that of modern superalloys. That is why the coating itself cannot bear the loads applied to the sample during its high-temperature strength testing carried out at temperatures above 700 °C. The stresses arising in the coating at the moment of the sample loading, as a rule, exceed the coating yield strength, so they are relieved and redistributed over the cross section of the superalloy. The stresses in the tested sample should be calculated taking into account the sample cross-sectional area, while the coating thickness is negligible.

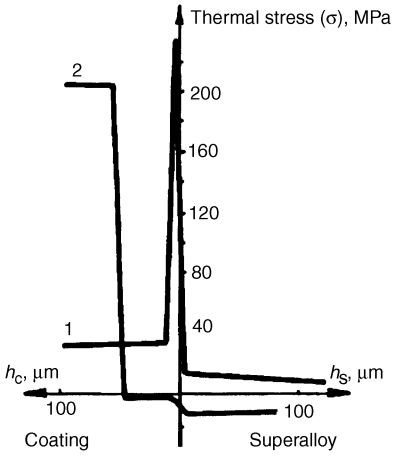

Fig. 7.16 Calculated thermal stresses at 20 °C in two-layer coatings on JS6F superalloy specimens [001]. 1, Ni20Cr12AlY (95 μm)/Ni8Co20Cr12AlY (5 μm); 2, Ni8Co20Cr12AlY (50 μm)/Ni20Cr12AlY (50 μm). h_c, distance from a "coating alloy" interface into the coating; h_s, distance into the alloy

The nature of the protective coating effect on high-temperature strength of nickel superalloys is closely related with the peculiarities of their failure in an oxidizing atmosphere at high temperatures. For a majority of the superalloys, oxidation at testing promotes the development of surface cracks and contributes to their damaging processes. Application of coatings that protect the surface of such superalloys from oxidation has a favorable effect on high-temperature strength, especially in the case of long-term testing.

At the same time, the coating may have a negative effect on high-temperature strength of the superalloy to be protected. This is due to the formation of an interaction zone that reduces the sample cross-sectional area, especially in the case of precipitation of laminated, closely packed phases (such as carbides, σ-phase).

The scope of testing carried out to evaluate the coating effect on high-temperature strength is great enough. However, the authors of most papers restricted themselves to comparison of the time-to-failure of the coated and uncoated samples. As a rule, in this case it is stated that coating deposition does not reduce sample time-to-failure.

Creep-Rupture Strength of Superalloys Tested in Media Provoking Hot Corrosion. Testing for creep and stress-rupture properties in a medium simulating fuel combustion products with elevated sulfur content substantially accelerates the failure processes occurring in the specimen surface layers and their destruction. The testing procedure was as follows (Ref 13, 14). The gas turbine fuel (GZT) synthetic ash was applied from an alcohol suspension to the surface of the standard specimens intended for high-temperature testing. The specimen was 6 mm in diameter, with the working part 30 mm long. The ash layer was 120 g/m^2, with the layer application repeated every 500 h of testing. Air supplied at a rate of 20 L/h was forced through the furnace muffle where the specimen was held for testing.

The results of the JS6U superalloy testing in air and with a layer of ash on it at 800 and 900 °C are shown in Fig. 7.17. The superalloy was considerably damaged during testing where the

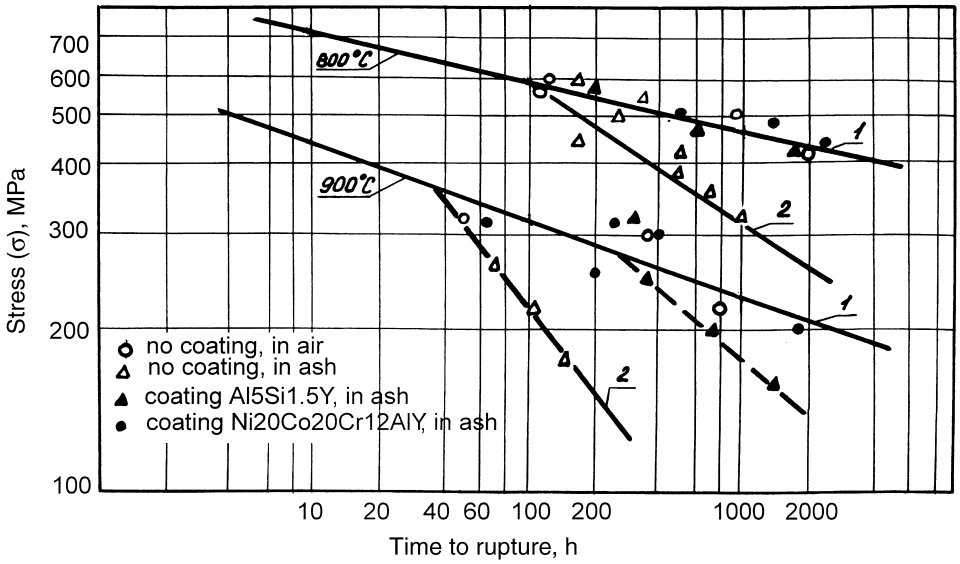

Fig. 7.17 Stress-rupture curves of JS6U superalloy in air (1, ○) and in GZT ash (2, △). Ni20Co20Cr12AlY coating (●) and diffusion coating (Al5Si1.5Y) (▲) in GZT ash

GZT ash was used. It manifested itself in an intensive time-dependent drop of the superalloy strength. In this case, the strength versus test time is still the same, both under hot corrosion conditions and in the air. It is an exponential equation establishing a relationship of time-to-failure to stress (Ref 13):

$$\tau = a \cdot \sigma^{-n}$$

where τ is time-to-failure, σ is stress, and a and n are constants depending on material properties, corrosive medium, and temperature.

At longer test time and higher test temperatures, the effect of the medium on the superalloy is greater, as is shown in Fig. 7.17 (Ref 15). After ~100 h of testing at 800 °C and 40 to 50 h at 900 °C, creep-rupture strength of the JS6U superalloy with the GZT ash starts to decrease. If the initial life of the JS6U superalloy in air is 1000 h, the GZT ash on it will reduce it by 74% at 800 °C and by 91% at 900 °C. The difference in high-temperature creep-rupture strength levels of the specimens tested in air and in the corrosive media becomes more pronounced as their testing time increases.

Table 7.14 Time-to-failure of JS6K superalloy in air and in GZT ash at the same stress level. (Ref 13)

Test temperature, °C	Stress (σ), MPa	Time to failure at testing in air (τ_A), h	Time to failure at testing in GZT ash (τ_{GZT}), h
800	410	1000	180
850	297		165
900	179		100
800	293	10,000	670
850	190		280
900	112		190

The same effect can be observed for the JS6K superalloy (Table 7.14). At long-term testing, time-to-failure decreases by a few orders of magnitude. The higher the test temperature is and the smaller the diameter of the specimen tested, the greater the medium effect will be.

In addition to shortening superalloy specimen lives under hot corrosion conditions, their initial, secondary, and tertiary creep lives become shorter, too; total ductility (specimen elongation) at failure and ductility at the initial and secondary creep phases are reduced. The JS6U superalloy behavior at testing is typical of all nickel superalloys.

Two test-coated JS6U and JS6K superalloys under corrosive conditions, two types of coatings were used: a diffusion coating made of the Al5Si1.5Y alloy deposited by the EA method and an overlay coating made of the Ni20Co20Cr12AlY alloy deposited by the EB method. The coating thickness values were ~50 and ~100 μm, respectively.

The test results on creep-rupture strength of the coated alloys under hot corrosion conditions

are shown in Fig. 7.17. The Ni20Co20Cr12AlY coating on the JS6U and JS6K superalloys guarantees their protection against hot corrosion as well as ensures their long-term strength characteristics similar to those typical of testing in air. The creep-rupture strength level of the coated JS6U superalloy at 2000 h testing at 800 °C is 400 MPa, while that for the uncoated specimen is 240 MPa. At 900 °C, the coating guarantees the alloy protection for more than 1000 h. In this case, the alloy high-temperature strength level is 220 MPa. At the same time, the uncoated alloy has creep-rupture strength of less than 100 MPa.

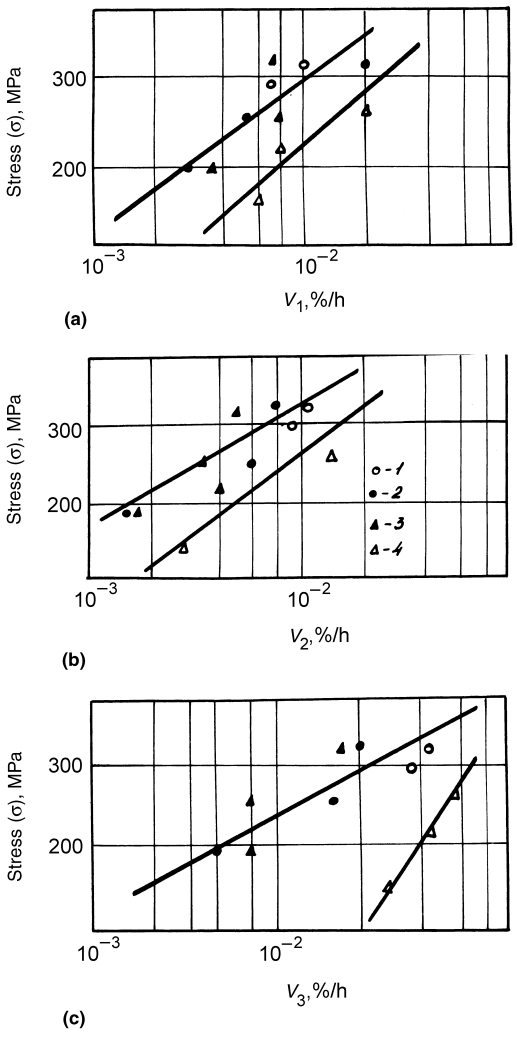

Fig. 7.18 Creep rates (V, %/h) of JS6U superalloy at 900 °C at (a) initial, (b) second, and (c) tertiary creep stages. 1, Air, no coating; 2, GZT ash, Ni20Co20Cr12AlY coating; 3, GZT ash, diffusion coating (Al5Si1.5Y); 4, GZT ash, no coating

Diffusion coatings demonstrate worse protective properties. However, they reliably protect the alloys against hot corrosion at 800 °C for at least 1000 h. The JS6U properties under these test conditions are the same as at its testing in air. At 900 °C, the diffusion coating becomes faulty after ~200 h, and a loss of creep-rupture strength is observed for the specimens with this coating. However, it is higher than that of the uncoated JS6U and JS6K superalloys.

The creep rate for the coated JS6U and JS6K superalloys when tested in the GZT ash is the same as at their testing in air (Fig. 7.18). In addition, the coated specimens do not lose their ductility (Fig. 7.19), as compared with the uncoated specimens tested under the same conditions.

The study of the nature of coating failure during testing has not revealed any peculiarities or distinctions from the failure of these coatings without any load applied. The size of the Ni20Co20Cr12AlY coating/JS6U superalloy interaction zone after 3000 h testing at 900 °C does not exceed 20 μm. The typical feature of the Ni20Co20Cr12AlY coating detected during testing is its high ductility. At testing, cracking occurs beneath the coating that is strained above the crack but is not faulty.

Creep-Rupture Strength of Superalloys Tested in Air. High-temperature testing of superalloys with directional solidification (DS) and single-crystal (SC) structures corroborates the general features revealed of the protective-coating effect on their high-temperature strength. The results of testing for creep-rupture strength of the directionally solidified JS26-DS superalloy with the Ni20Co20Cr12AlY coating are shown in Fig.7.20. At testing at 1100 °C for 1000 h, creep-rupture strength values for the coated and uncoated specimens are 55 and 45 MPa, respectively. The mismatch between creep-rupture strength of the coated and uncoated alloys is much less than that obtained at testing in the GZT ash medium and than could have been expected from the uncoated alloy oxidation depth.

No evidence of the expected effect is likely to result from the fact that under high-strain conditions typical of the specimens with directional structures, the surface crack-growth rate exceeds the specimen oxidation rate. Despite coating ductility and protection of the alloy against oxidation, some cracks develop beneath the coating, too (Fig. 7.21). The cracks gradually propagate and cause damage to specimens.

The development of interaction processes between the coating and the alloy leads to a decrease of the specimen cross-sectional area. Dissolution of the γ'-strengthening phase in the interaction zone beneath the coating reduces the alloy strength. As a result, the working cross-sectional area of the JS-type superalloy specimen 5 mm in diameter is reduced by 5 to 7% after 500 h of testing. It is much less than in the case of oxidation effect. Yet, for the blades less than 2 mm thick and bearing high loads, the effect of interaction between the coating and the superalloy should be taken into account.

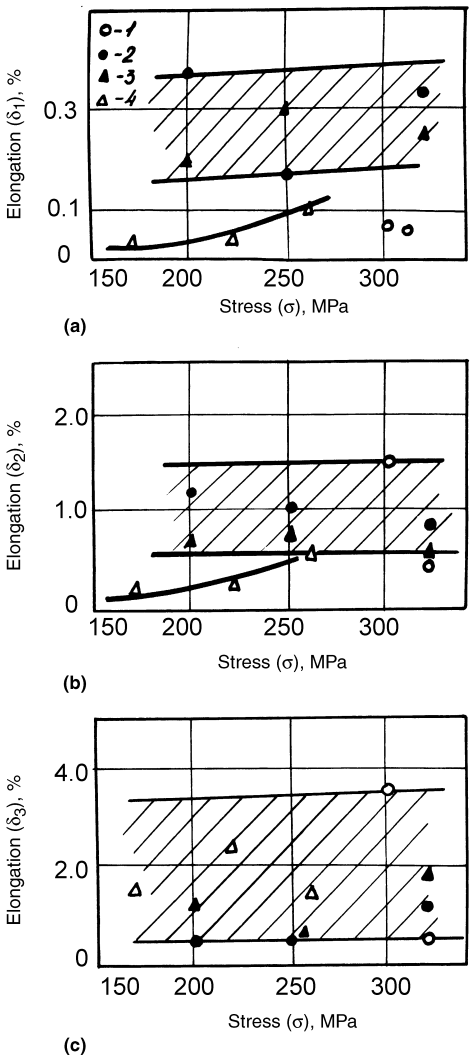

Fig. 7.19 Relative elongation of JS6U superalloy at 900 °C versus stress at (a) initial, (b) second, and (c) tertiary creep stages. 1, Air, no coating; 2, GZT ash, Ni20Co20Cr12AlY coating; 3, GZT ash, diffusion coating (Al5Si1.5Y); 4, GZT ash, no coating

The structural investigations do not reveal differences in the interaction zone between coatings and the superalloys tested under no-load conditions and with high stresses and strains applied. It is explained by the fact that the energy contribution to the diffusion processes due to high temperatures substantially exceeds the energy contribution of the stresses.

In all the nickel superalloy specimens tested at long-term static loading, the initial failure zone is located on the specimen surface, which points to similar failure patterns based on crack development and propagation causing destruction at the final creep stage. The coating does not change the failure mechanism; it only neutralizes the effect of oxidation on it.

Mechanism of Coating Effect on Superalloy Creep-Rupture. Summarizing the experimental data on the coating effect on high-temperature strength of superalloys, the following conclusion can be drawn. The plot of stress level as a function of time-to-failure that is a straight line has a point corresponding to a certain test time of τ_c (Fig. 7.22). Starting from this moment, the uncoated specimens start losing their creep-rupture strength due to oxidation effect, surface softening, and reduction of their cross-sectional areas. Starting from this moment, creep-rupture strength of the specimens with coatings that protect their surface against oxidation, softening, and respective reduction of their cross-sectional areas is higher in comparison with that of the uncoated specimens.

Time of τ_c is a measure of an uncoated specimen test life. Testing for a longer period should be carried out only on protected specimens. The τ_c point position depends on heat resistance of the alloy tested, test temperature, environment aggressiveness, and the diameter of the specimen tested.

Time of τ_c for specimens 5 mm in diameter and made of heat-resistant superalloys (such as JS6K, JS6U, JS32, etc.) tested in air at 900 to 1000 °C is more than 1000 h. That is why most investigators do not reveal a positive effect of coatings on creep and stress-rupture properties of these alloys, because they reduced their test time to 100 to 500 h. A more aggressive medium, elevated temperatures, smaller specimen diameters, and reduced heat resistance shift the τ_c point to the left. When testing the JS6U superalloy in the GZT synthetic ash medium at 800

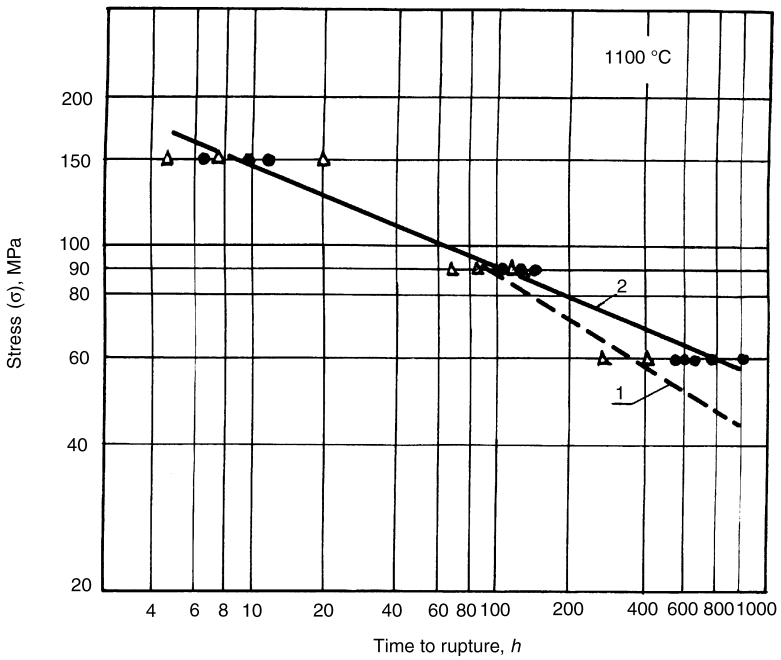

Fig. 7.20 Stress-rupture curves of JS26-DS alloy in air at 1100 °C. 1, Δ, No coating; 2, ●, Ni20Co20Cr12AlY coating

and 900 °C, the τ_c time values are 100 and 500 h, respectively.

Effect of Coatings on Fatigue Strength of Superalloys

One of the factors that may cause turbine-blade failure is blade-material fatigue. Fatigue cracks usually develop in the blade surface layer in the zone of the greatest alternate stress effect. Blade fatigue strength depends on the surface condition and can vary substantially when a coating with physical and mechanical properties different from those of the superalloy is applied. At testing for fatigue, it is necessary to take into account the fact that the coating effect manifests itself clearly during bend-testing when the maximum strain area is located on the surface. The following factors have an effect on fatigue strength of coated specimens:

- Coating structure (defects, texture, grain size and orientation, and phase composition)
- Coating thickness and ratio of coating thickness and specimen cross-sectional area
- Structure of the coating-alloy interaction zone (presence of needlelike precipitate of closely packed phases)
- Sign and level of thermal stresses in the coating
- Coating-material fatigue strength
- Coating surface roughness

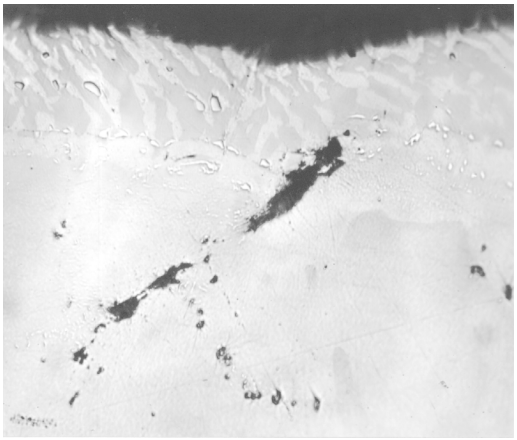

Fig. 7.21 Surface microstructure of JS26-DS superalloy sample with Ni20Co20Cr12AlY coating after testing for stress-rupture strength. Applied stress (σ) = 150 MPa; time to rupture (τ) = 22 h. 300×

Fatigue Strength of Superalloys with Diffusion Coatings. Both thermal stresses generated in diffusion coatings and strength and ductility differ substantially from the respective properties of overlay coatings. As a result, the

effect of these two groups of coatings on superalloy fatigue strength is different.

The results of extensive studies of fatigue strength of superalloys with diffusion aluminide coatings revealed the following main relationships.

In the temperature range of 20 to 250 °C, fatigue strength of the specimens with diffusion coatings is higher than that of unprotected specimens (Ref 16, 17). The increase in fatigue strength depends on the coating chemical composition, the alloy properties, and the thickness of the specimens tested. This effect of diffusion coatings is explained by substantial compressive stresses (-150 to -300 MPa) in them. These stresses compensate for the low strength and zero ductility of coatings in the temperature range in question.

Testing at high stresses when tensile stresses arise in the surface layer may cause cracking even at the first stages of testing. Such cracking reduces total service lives of the specimens with diffusion aluminide coatings compared to the uncoated alloy in the range of 20 to 250 °C.

At 900 to 950 °C, no deterioration of fatigue strength of the specimens and blade models made of the JS6K and JS6U superalloys and protected with diffusion coatings has been detected compared with unprotected specimens (Ref 18, 19).

Oxidizing protected and unprotected specimens before testing under the air atmosphere at 950 °C for 1000 h reveals the positive effect of the applied coatings. Depending on the test time, preoxidation of the uncoated samples results in the reduction of the JS6K superalloy sample fatigue lives by 10 to 17%. Fatigue lives of the samples with the diffusion coatings also decrease, although this reduction is 5 to 12% and also depends on the test time. Thus, fatigue lives of the coated samples are higher than those of uncoated samples by 6 to 9%. Similar results were obtained on testing the blades.

Reduction of sample fatigue lives at long-term testing in the high-temperature range under oxidizing atmospheres results from two processes: changes in superalloy structure and sample surface oxidation. For the uncoated sample, its fatigue life drop is the consequence of more intensive oxidation of its surface and softening of its surface layer.

The same effect of diffusion coatings has been revealed at testing in an aggressive medium of fuel combustion products (Ref 20). Test results for blade models with edge radii of 0.5 mm and made of the Ni10CrWMoCo alloy are presented in Fig. 7.23. The tests were carried out under conditions of asymmetrical bending for the samples supported as a cantilever (cycle stress range $\sigma_m = 200$ MPa) in the T-1 aircraft fuel combustion products. The test temperature was 900 °C, its cycle vibration frequency was 50 Hz, and test time provided for 10^6 to 10^7 cycles. The diffusion coating was applied to the samples from the powder mixture of 98% Al-Fe alloy (50% Al) and 2% NH_4Cl at 950 °C. The coating thickness was 50 μm; its aluminum content was 34 to 36%.

In corrosive media, diffusion coatings on blade models guarantee a fatigue-strength level 25 to 30% higher than that of the uncoated specimens. The JS6K and JS6U superalloys showed the same results. Favorable outcome of fatigue-strength testing of blades with diffusion coatings

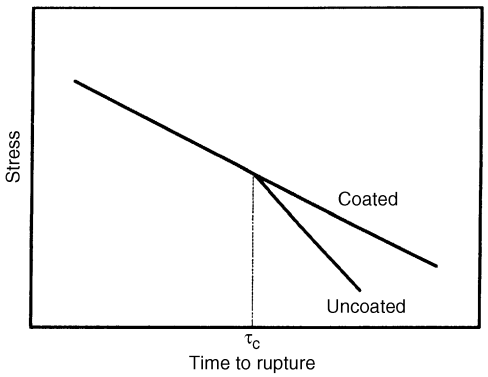

Fig. 7.22 Diagram illustrating the effect of coatings on creep-rupture strength of superalloys

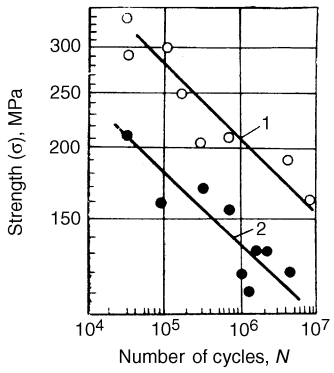

Fig. 7.23 Fatigue strength of blade models made of JS6U superalloy. Testing in combustion products of T-1 aircraft fuel at 900 °C. 1, diffusion-coated samples; 2, uncoated samples

was also observed after their service in engines (Ref 21).

Fatigue Strength of Superalloys with Overlay Coatings. Fatigue-strength testing of superalloys with different modifications of overlay coatings in the temperature range of 20 to 1100 °C (Ref 22, 23) has revealed the following relations.

At temperatures lower than 500 °C, tensile stresses arise in the surface layers of the specimens with overlay coatings. Their values depend on the coating chemical composition. Ultimate and yield strength values of overlay coatings are rather high in this temperature range. They are higher than the stresses applied to the specimens during testing. Under these conditions, no increase in fatigue strength, which is typical of diffusion coatings, is observed.

When testing round, standard specimens 8 mm in diameter with the Ni20Cr12AlY coating 60 μm thick under pure bending conditions at 20 °C, no decrease in fatigue strength is detected (Table 7.15). As a rule, a single crack that causes failure (Fig. 7.24) appears on the specimen surface. The site of failure is located on the coating surface. The same results were obtained on the specimens made of the JS6F, JS26-DS, and JS32-DS superalloys.

At 20 °C, an insignificant rise in fatigue strength is noted on round specimens made of the VJL12U superalloy with the working part 3 mm in diameter and the Ni20Cr12AlY overlay coating 100 μm thick (Fig. 7.25). It may result from the fact that on testing the specimens 3 mm in diameter, their stresses were calculated by ignoring coating thickness contribution to their cross-sectional areas.

Fatigue-strength testing of finished blades at 20 °C is a mandatory check operation in blade-lot manufacturing at the plants. Heat treatment of the blades and machining of their surfaces have an important effect on the reference values of blade fatigue strength (Table 7.16). Fatigue life of the blade with a diffusion coating at the test stress of 180 MPa is more than $N = 2 \cdot 10^7$ cycles. When the Ni20Cr12AlY overlay coating is applied instead of a diffusion coating, reduction of fatigue life to $N = 6 \cdot 10^6$ cycles is observed. Peening with microballs and generation of high-level compressive stresses did not extend blade lives, although the site of failure shifted to their inner-cavity surface. The initial blade-fatigue life was obtained again after reducing the temporary annealing temperature to 1000 °C.

At 20 °C, the defects of an overlay coating, such as intercrystalline porosity, microdrops, and so on that cause stress concentration, are the sites of fatigue-crack nucleation. These blade defects in the zones of high alternate stresses are prohibitive.

At temperatures above 700 °C, overlay coatings are free from stresses or show low compressive stresses. During fatigue-strength testing, the stress level on the specimen surface considerably exceeds coating yield strength and ultimate strength. The effect of combined strains, depending on the superalloy mechanical properties and test conditions, causes an accelerated accumulation of ductile strain followed by a respective accumulation of defects. The process is more intensive in the coating than in the bulk superalloy. It results in the formation of fatigue cracks and, as a rule, the cracks are not longer than the coating thickness.

The results of fatigue strength testing of the JS6U superalloy with the Ni20Co20Cr12AlY and Ni20Cr12AlY coating at 950 °C are given in Table 7.15. Fatigue strength tested on the basis of $2 \cdot 10^7$ cycles for the coated samples was the same as fatigue strength for the uncoated samples. The lack of a wholesome effect of the overlay coating is due to the fact that the rather short test time of ~120 h does not allow the effect of oxidation that reduces fatigue strength of uncoated samples to be noticed. Similar results were obtained for other superalloys. On testing the coated samples 3 mm in diameter at 950 °C, a slight increase in fatigue strength was observed as compared with uncoated samples (Fig. 7.25).

The salient feature of high-temperature testing of specimens with diffusion and overlay coatings is the presence of numerous cracks on their surfaces (Fig. 7.26). These cracks are stress concentrators and cause formation of numerous sites of fatigue failure beneath the coating. Further crack propagation depends on the failure mechanism typical of the alloy tested at high

Table 7.15 Fatigue strength, σ_{-1}, of JS6U superalloy specimens 7 mm in diameter at 20 and 950 °C

	σ_{-1}, MPa ($N = 2 \cdot 10^7$ cycles)	
Coating	20 °C	950 °C
Uncoated	190	280
Ni20Cr12AlY	…	280 (δ = 100 μm)
Ni20Co20Cr12AlY	190 (δ = 60 μm)	300 (δ = 120 μm)

temperatures and on the specimen shape. Numerous surface sites merge and form a circular crack, thereby reducing the specimen cross-sectional area. However, this reduction of the cross-sectional area is insignificant for specimens 7 mm in diameter and does not affect their fatigue strength. The main site causing failure of the round specimens is located at a distance of 0.2 to 0.8 mm from the surface (Fig. 7.26c).

Studies of fatigue strength of superalloys with EB thermal barrier coatings (TBC) (the coating design is as follows: inner layer/intermediate layer/outer layer of Ni20Cr6AlY/Ni20Cr12AlY/ZrO_2-8%Y_2O_3, 35/45/60 μm thick, respectively) were carried out for two types of specimens. Round SC specimens 7 mm in diameter and made of the JS32-DS superalloy were tested under clear-bending conditions at 1100 °C. Flat specimens with thickness varying from 2 to 5 mm and made of the JS6U superalloy were bend-tested at 975 °C. Bending vibrations were exhibited in a magnetostrictor at a frequency of 3200 Hz.

The study of the nature of alloy round sample failure has confirmed the general features stated previously. The application of a TBC to a sample surface results (as has been observed for the Ni20Cr12AlY coating) in nucleating numerous sites of failure, followed by cracks propagating into the coating and further into the alloy. However, the main site of nucleation of the crack causing a sample failure is located beneath the coating surface at a depth of 1 to 1.5 mm, and it does not result from the coating effect. At 1100 °C, fatigue strength (on the basis of $N = 2 \cdot 10^7$ cycles) was $\sigma_{-1} = 150$ MPa. The presence of a ceramic layer changed neither the nature of sample failure nor fatigue strength values.

The situation changes on testing sheet (flat) samples (Fig. 7.27). In this case, the surface site of failure forms in the TBC in the maximum stress zone in the corner of the flat sample. The corner is a stress concentrator; it is the site from where the fatigue crack causing failure propagates. In this case, fatigue strength after $N = 1 \cdot 10^8$ cycles diminishes by ~30 MPa in comparison with unprotected samples, and the TBC has the same effect as the Ni20Cr12AlY coating lacking a ceramic layer.

Mechanism of Coating Effect on Superalloy Fatigue Strength. Fatigue-strength tests showed that the effect of overlay coatings on this superalloy property was different in the high- and low-temperature ranges.

At room temperature, the level of coating strength and respective fatigue strength approaches that of superalloys. That is why, despite tensile thermal stresses in the coating, sample and blade fatigue strength values do not actually change when overlay coatings are deposited. On testing small-sized (≤3 mm) samples, deposition of a coating 100 μm thick, which has high strength characteristics, can result in upgrading the level of fatigue strength.

On bend-testing in the low-temperature range, coating defects act as stress concentrators. If the coating is not free from defects, the sample and blade fatigue strength values may decrease.

At temperatures above 800 °C, overlay coating strength and respective fatigue strength are substantially lower than superalloy fatigue

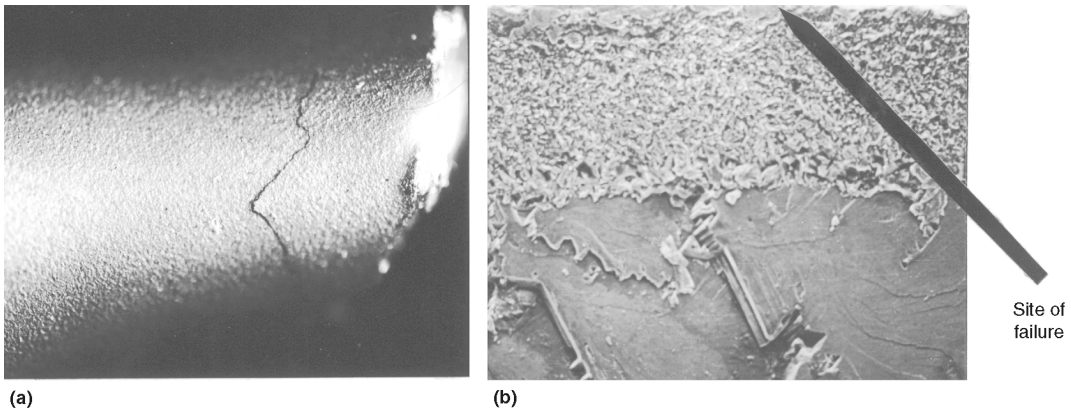

Fig. 7.24 (a) Appearance and (b) fracture of JS6U superalloy specimen with Ni20Cr12AlY coating. Specimen tested at 20 °C. σ = 200 MPa; $N = 1.8 \cdot 10^7$ cycles

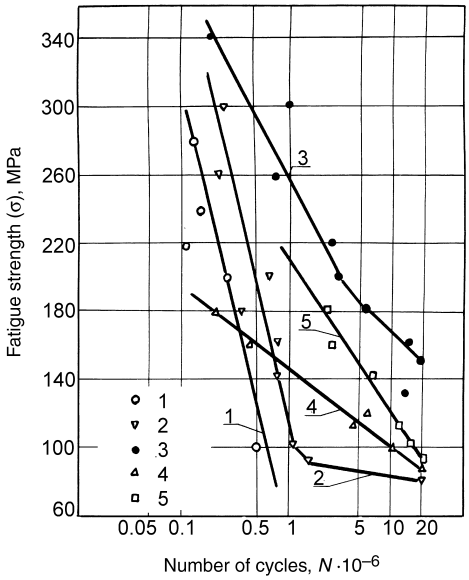

Fig. 7.25 Fatigue strength of VJL12U superalloy (3 mm bars). 1 and 2, 20 °C; 3, 700 °C; 4 and 5, 900 °C; 1 and 4, uncoated; 2, 3, and 5, Ni20Cr12AlY coating

strength. The coating quickly accumulates defects, and numerous fatigue cracks, which are effective stress concentrators, develop in it. In addition, the cracks open the access of oxygen to the alloy surface.

Further sample damage depends on the temperature, alloy heat resistance, sample shape, and medium aggressiveness. The amount of oxygen passing through the cracks to the alloy surface is much less than if there is no coating at all. The efficiency of the coating cracks as stress concentrators, taking into account the high ductility of the coating, does not exceed the efficiency of stress concentrators formed due to oxidation. In addition, when testing round samples under clear-bend conditions, a site of failure is formed, as a rule, beneath the surface and inside the sample. That is why on testing in the air at 900 to 1000 °C for $N = 2 \cdot 10^7$ cycles (~120 h), the values of fatigue strength for coated and uncoated samples are the same. In the case of testing in aggressive media, the coated samples have higher fatigue strength in comparison with uncoated samples.

The fatigue-strength testing procedure has much in common with testing for creep-rupture strength. A certain number of cycles, N_c, corresponds to the test time of τ_c (Fig. 7.22). On a lapse of these cycles, surface damage caused by oxidation and hot corrosion results in deterioration of uncoated sample fatigue strength. The values of fatigue strength for coated samples are higher than those for uncoated ones after the said number of cycles.

At temperatures of 900 to 1000 °C, heat resistance of the JS6U, JS6K, and VJL12U superalloys is rather high, and, in fact, their surfaces remain free from oxidation products after the said $N = 2 \cdot 10^7$ cycles (~120 h). That is why no effect of the coating on fatigue strength has been noticed in the tests carried out. However, when blades are used in turbines, the degree of their surface damage substantially exceeds the degree of sample surface damage at their testing for fatigue strength. That is why fatigue strength of the uncoated blades used in the engines is always lower than that of the coated blades.

Effect of Coatings on Thermal Fatigue of Superalloys

The blade designs featuring the most-effective cooling systems, the increase in temperature gradients through the blade-wall thickness, and the nonuniform temperature fields over the blade surfaces have resulted in the growth of thermal fatigue cracking events in the coatings. That is why the study of coating effect on superalloy resistance to failure during their heating and

Table 7.16 Fatigue strength of JS6U superalloy blades at 20 °C

Stresses on leading edge	Number of test cycles before cracking	Location of cracks	Type and characteristics of coating and technological process
180 MPa	$>2 \cdot 10^7$	Inner cavity at leading edge where stresses are accumulated	Diffusion coating, 40 μm thick, annealing: 1000 °C, 4 h
180 MPa	$6 \cdot 10^6$	Outer surface of loading edge where it develops into shroud	Ni20Cr12AlY coating, 100 μm thick, annealing: 1040 °C, 5 h
180 MPa	$(8 \div 15) \cdot 10^6$	Inner cavity at leading edge where stresses are accumulated	Ni20Cr12AlY coating 100 μm thick, annealing: 1040 °C, 5 h; peening
180 MPa	$>2 \cdot 10^7$	Cracks are not detected	Ni20Cr12AlY coating 100 μm thick, annealing: 1000 °C, 5 h

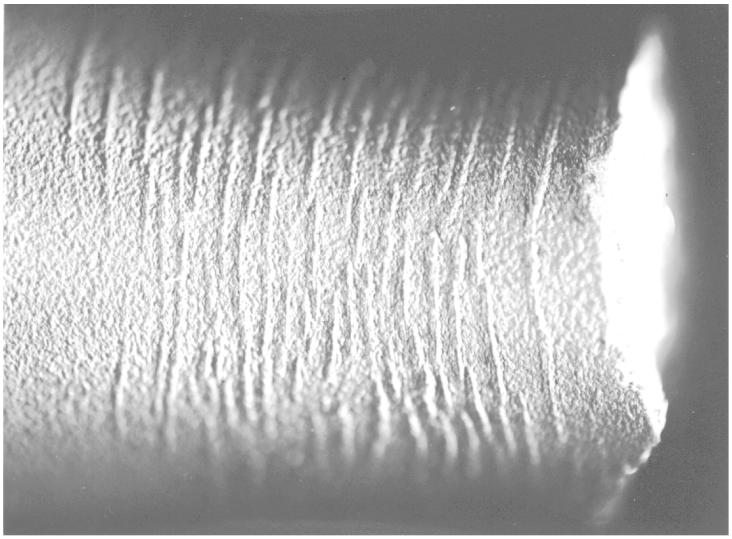

(a)

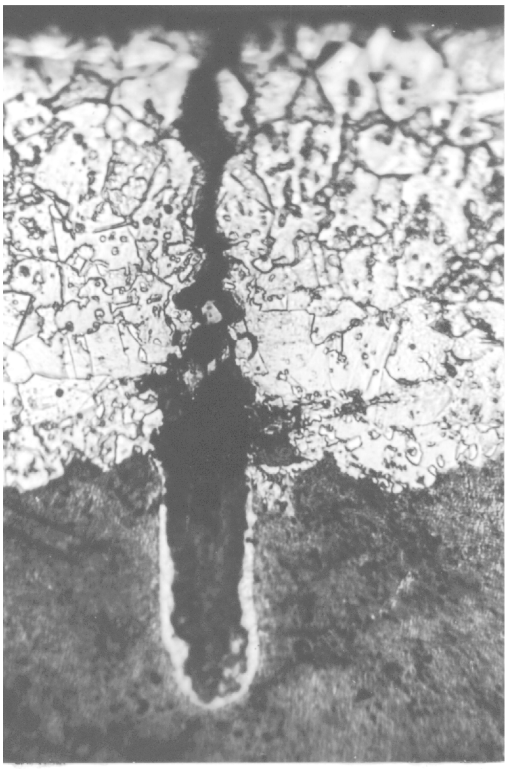

(b)

(c)

Fig. 7.26 (a) Appearance, (b) microstructure, and (c) fracture of JS6U superalloy specimen with Ni20Cr12AlY coating. Specimen tested at 950 °C. $\sigma = 300$ MPa, $N = 2.4 \cdot 10^7$ cycles

cooling cycles is an important point in the investigation of the properties of the coatings designed to protect turbine blades. Numerous publications deal with this problem.

A complicated dependence of thermal fatigue on test rig parameters and on the structural design of the blades and test samples, as well as the lack of a single-valued criterion for thermal fatigue estimation, to some extent, make interpretation of numerous test results more complicated. Resistance of blades and samples to thermal fatigue depends on mechanical and thermal-physical parameters of the materials, such as strength, ductility, elasticity modulus, thermal expansion coefficient, and thermal conductivity. The test conditions, which have a great effect on thermal fatigue characteristics, are as follows: rates of heating and cooling, cycle maximum and minimum temperatures, holding time at the maximum temperature, and static loads applied.

During thermofatigue testing of the blades and samples, their surfaces interact with gaseous atmosphere. As a result of this interaction, the top layers of the metal are depleted of alloying elements. This reduces a fraction of strengthening phases in them and degrades their high-temperature strength. The changes in the chemical composition of the surface zone and the respective variations of thermal expansion coefficients result in an additional increasing of thermal stresses. They can reach a level considerably exceeding the surface zone strength. Thermal fatigue cracking in the surface zone followed by crack propagation into the base material resulted in test sample failure.

The presence of heat-resistant coatings on sample or blade surfaces, which protect the base material against oxidation and softening, is expected to have a favorable effect on resistance to thermal fatigue. In this case, physical-mechanical and thermophysical characteristics of the coating have a substantial effect on the test results.

As a rule, rigidity of coatings ($E_c \cdot h$) is much less than that of a blade wall or a sample ($E \cdot H$):

$$\frac{E_c \cdot h}{E \cdot H} < 0.1$$

where E_c and E are the coating and superalloy elasticity modulus, respectively, and h and H are the thickness of a coating and a blade wall or a sample.

Under these conditions, even at slow cooling or heating of the sample with the coating deposited at the temperature of T_0, thermal stresses arise in the coating. Under the conditions of long-term cycling and accumulation of the strain induced by thermal stresses, thermal fatigue cracking may occur even if no additional stresses are generated by impressed forces.

Thermal stresses may vary in the coating if a temperature gradient in the coating/blade-wall zone arises. It is always present in cooled blades and substantially rises at turbine transient power settings. If the sample or blade construction is stressed or strained because of their nonuniform temperature pattern along its full height and surface, coating thermal stresses are added to structural thermal stresses.

As a rule, thermal fatigue tests are carried out on gas-dynamic test rigs at alternating heating-cooling cycles. Test results depend on specimen shape, stiffness and rigidity, maximum and minimum cycle temperatures, rates of heating and cooling, and gas parameters and composition. Under these test conditions, thermal stress and strain values in the specimens may be controlled by specimen rigidity (e.g., solid or hollow specimens, etc.), rates of heating and cooling, and maximum and minimum cycle temperatures.

Thermal fatigue is characterized by the number of cycles to appearance of the crack of the specified size on the specimen surface. This characteristic, to a considerable extent, is a qualitative one. It may be used for revealing the advantages of a certain blade construction or a certain superalloy or protective coating. However, this characteristic cannot be used for blade service-life calculations. In addition, as a rule, gas-dynamic test rigs do not simulate heat flows typ-

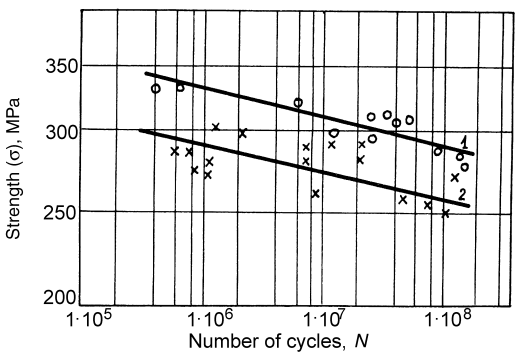

Fig. 7.27 Fatigue strength of JS6U superalloy (1) without any coating and (2) with EB-TBC

ical of the engines. That is why the results of the rig tests cannot reveal the features of coating behavior on the cooled blades at very high rates of their heating and cooling that occur under transition working conditions in modern engines.

Proceeding from extensive testing results for specimens with different aluminide coatings, it is noteworthy that aluminum content of the coating outer zone and the coating thickness are the main factors that have an effect on the test results. The reduced aluminum content of the coating involving the respective reduction of the NiAl compound ductile-brittle transition temperature improved thermal fatigue resistance of the specimens and blades with diffusion aluminide coatings. The reduction of coating thickness had the same effect.

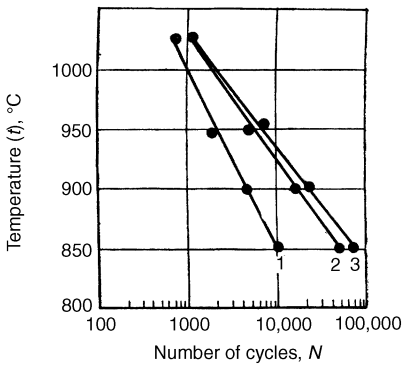

Fig. 7.28 Thermal fatigue resistance of JS6K superalloy blades versus maximum cycle temperature. 1, Uncoated; 2, diffusion coating of aluminum, Al_2O_3, and NH_4Cl mixture; 3, diffusion coating of aluminum, chromium, Al_2O_3, and NH_4Cl mixture. Source: Ref 24

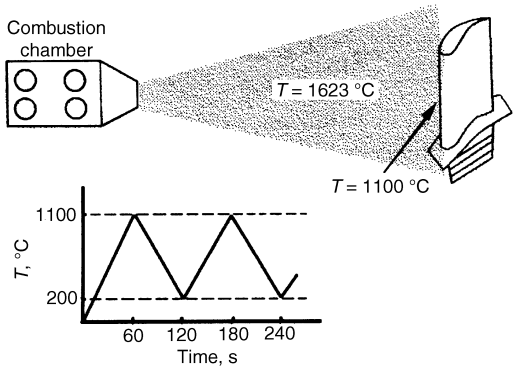

Fig. 7.29 Schematic diagram of test rig for thermal fatigue tests

On setting up the program for testing specimens with diffusion coatings, it is necessary to take into account some specific coating features, such as low ductility of the coatings with the aluminum content of more than 32% and gradual aluminum content reduction during testing, followed by the increase in coating ductility. Crack nucleation may take place in a diffusion coating with high-aluminum content even after the first few heating-cooling cycles at testing for thermal fatigue under conditions of high thermal stresses and respectively high strains. On running the same tests for the coated specimens with low-aluminum content of the coating, their cracking occurs much later than in uncoated specimens.

Typical results of testing for thermal fatigue of aluminized blades made of the JS6K superalloy on the gas-dynamic test rig are presented in Fig. 7.28 (Ref 24, 25). The maximum gas temperature available in the test rig is 1500 °C, the time of heating to the preset temperature is ~8 s, and the cooling time is ~17 s. The maximum test temperatures were 1000, 950, 900, and 850 °C. The minimum cycle temperature was ~300 °C. After every 100 cycles, the specimens were examined visually for crack detection.

Under the conditions of the tests carried out, the aluminized coatings increased thermal fatigue resistance. Under the conditions of 850 ⇔ 300 °C cycling, aluminized blades withstood ~4 times as many cycles to crack nucleation as uncoated blades. The increase in the maximum cycle temperature followed by the respective increase in thermal stress and strain values resulted in less difference in thermal fatigue resistance of coated and uncoated blades.

The addition of salt to the gas flow under the same test conditions gives rise to hot corrosion and reduces blade service life considerably. However, in all cases, the service lives of the blades with aluminized coatings are longer than those of uncoated blades.

Experimental Studies of Coated Superalloy Thermal Fatigue. A large body of information on comparison tests for specimens and blades with different coatings is received using the gas-dynamic test rig. Its layout is given in Fig. 7.29.

Knife-edged solid and hollow samples with an edge radius of 1 mm (Fig. 7.30) are used for testing. Eight samples are simultaneously fastened in the special fixtures of the test rig. Then, they are moved in turn into a combustion chamber, where they are heated to 1000 or 1100 °C,

and to compressed air supply systems, where they are cooled to 200 °C. The combustion chamber uses aircraft fuel. The preset program may change the cycle duration. Two options of the cycle were used for testing:

- $\tau_{heat} = \tau_{cool} = 30$ s
- $\tau_{heat} = \tau_{cool} = 30$ s, holding time at the cycle maximum temperature of 60 s

The second option was intended to determine coating resistance to thermal fatigue at surface exposure to severe conditions caused by oxidation.

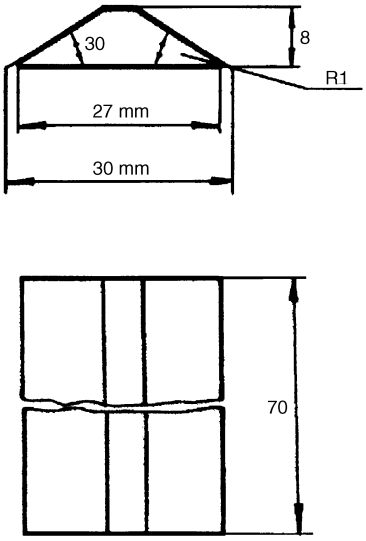

Fig. 7.30 Sketch of specimens for thermal fatigue tests. R1, radius equal to 1 mm

Table 7.17 Test conditions

No.	Temperatures	Time
1	1000 °C ↔ 200 °C	Time required for heating the sample to the maximum temperature is 30 s; cooling time is 30 s
2	1000 °C ↔ 200 °C	Time required for heating the sample to the maximum temperature is 30 s; holding time at the maximum temperature is 60 s; cooling time is 30 s
3	1100 °C ↔ 200 °C	Time required for heating the sample to the maximum temperature is 60 s; cooling time is 60 s
4	1200 °C ↔ 200 °C	Time required for heating the sample to the maximum temperature is 60 s; cooling time is 60 s
5	1000 °C ↔ 200 °C	Time required for heating the sample to the maximum temperature is 120 s; cooling time is 120 s

Within the first seconds of heating hot gases from the combustion chamber, heat the sample central portion that is not large (20 to 30 mm). It gives rise to a temperature gradient through its full length and thickness. This gradient induces thermal stresses and strains, which peak on the sample edge with a radius of 1 mm that faces the flow of heating and cooling gases. Strain accumulating in this place causes thermofatigue cracking of the sample. The number of cycles to development of a crack ~0.5 mm long on the edge of the sample is its life criterion. Test conditions used are given in Table 7.17.

The test results are given in Table 7.18 and shown in Fig. 7.31. When testing uncoated samples of the JS6U superalloy at the cycle maximum temperature of 1000 °C, accelerated oxidation of their working edges and surfaces is observed. Numerous cracks nucleate in these zones. Protective coatings of all compositions protect the superalloy surfaces against oxidation and softening and, thus, increase the number of cycles to thermal fatigue cracking. A narrower range of strains arising on a hollow sample in comparison with the solid one leads to a cyclic life of ~1.2 times as long.

The sample holding time at the cycle maximum temperature has a substantial effect on the test results. The development of creep at a high temperature and oxidation of coating surfaces encourages accumulation of strains and facilitates a failure of both the coating and the superalloy. The samples tested at a holding time at the maximum temperature of 60 s feature cyclic lives 1.5 to 3 times shorter in comparison with those of the samples tested without the high-temperature holding.

Under long-term cycling conditions (120 s), the distinctions caused by sample physical-mechanical characteristics diminish. Cyclic life of a JS6U superalloy sample with an overlay coating is ~1.2 times longer than that of a sample with a diffusion coating, while at testing under short-term cycling conditions, the respective parameter is 2.2.

Thermal fatigue of the coated samples, which are thermally stressed on the test rig under consideration, is closely related with both high-temperature properties of the alloys and sample fabrication techniques. The test results for the samples made of the JS6U superalloy (equiaxial solidification), the JS6F-DS superalloy (direc-

tional solidification), and the JS30-SC (single crystal) with the diffusion aluminized coating deposited from a mixture of 98% of the Al-Fe (36% Al) alloy and 2% NH_4Cl are presented in Table 7.18. The aluminum content of the coating outer zone is ~22 to 24%; the coating is 30 to 50 μm thick. According to their resistance to thermal fatigue, the alloys are ranged as follows: JS6U (1), JS6F-DS (1.35), and JS30-SC (1.45).

Better ductility and strength of coatings as well as a smaller mismatch between TECs of a coating and a superalloy increase sample service lives and reduce the distinction of thermal fatigue for superalloys with different structures. The same alloys tested with the Ni20Cr12AlY/Ni10Co20Cr12AlY coatings 100 μm thick deposited by EB technique have the same cyclic lives: JS6U (1), JS6F-DS (1), and JS30-SC (1). This is explained by the fact that long-term cycling gives rise to the accumulation of damages not in a superalloy but in a coating, in the zone of maximum oxidation and thermal strain effect.

On testing the samples made of the JS6U superalloy at long-term cycling (120 s) for their resistance to thermal fatigue, the coatings are ranged as follows: aluminized coating (1), (Al5Si1.5Y) diffusion coating (1.10), Ni20Cr12AlY coating (1.20), and Ni20Co20Cr12AlY coating (1.30). The same testing under short-term cycling conditions (60 s) gives the following ranges: aluminized coating (1), Ni20Cr12AlY coating (2.25), and Ni20Cr12AlY/Ni10Co20Cr12AlY coating (2.40). Longer cyclic lives of the samples with the Ni20Cr12AlY/Ni10Co20Cr12AlY coating are due to their better surface roughness characteristics and fewer number of defects in the coating structure when the two-stage surface preparation technique is used, which is described in Chapter 3, "Phase Composition of Coatings on Superalloys."

The surface study of the samples tested on a gas-dynamic test rig has shown that the nature of their failures is similar in all cases; that is, numerous thermal fatigue cracks develop on the working edge at a distance of 0.6 to 1.0 mm from one another, and the crack edges are open and oxidized. Depending on coating ductility, the cracks either propagate perpendicularly to the surface or their abundant branching is observed in the coating.

Table 7.18 Number of cycles (*N*) to cracking for hollow samples at their testing for thermal fatigue on 8UTS test rig

Superalloy	Coating	Deposition method	Thickness, μm	Test condition	N_C
JS6U	Uncoated	…	…	1	1190
JS6U(a)	Uncoated	…	…	2	580
JS6U	Aluminized	Aluminizing	40	1	1610
JS6U(a)	Aluminized	Aluminizing	40	2	830
JS6U	Aluminized	Aluminizing	40	2	1010
JS6U	Al5SiY	EA	40	2	1080
JS6U	Ni20Cr12AlY	EB	100	1	3680
JS6U	Ni20Cr12AlY	EB	50	2	1160
JS6U	Ni20Cr12AlY	EB	100	2	1210
JS6U	Ni20Cr12AlY/Ni10Co20Cr12AlY	EB	20/80	1	4720
JS6U	Ni20Co20Cr12AlY	EB	100	2	1310
JS6U	Ni20Co20Cr12AlY	EB	100	5	1330
JS30-SC	Uncoated	…	…	1	2200
JS30-SC	Aluminized	Aluminizing	40	1	2420
JS30-SC	Ni20Cr12AlY/Ni10Co20Cr12AlY	EB	40/60	1	4030
JS6F-DS	Uncoated	…	…	1	1900
JS6F-DS	Aluminized	Aluminizing	40	1	2260
JS6F-DS	Ni20Cr12AlY/Ni10Co20Cr12AlY	EB	40/70	1	4000
VJL12U	Al5SiY	EA	40	2	700
VJL12U	Ni20Cr12AlY	EB	50	2	740
VJL12U	Ni20Cr12AlY	EB	100	2	860
VJL12U	Ni20Co20Cr12AlY	EB	100	5	870
JS26-DS(a)	Ni20Cr12AlY/Al	EB/aluminizing	100	4	620
JS30-SC(a)	Uncoated	…	…	3	1190
JS30-SC(a)	Aluminized	Aluminizing	50	3	1300
JS30-SC(a)	TBC	EB	180	3	1530
JS32-DS(a)	Uncoated	…	…	3	1320
JS32-DS(a)	TBC	EB	180	3	1510

(a) Solid samples

The maximum range of thermal stresses and strains in a coating at lab testing can be reproduced on rapid cooling of heated samples in cold water. In this case, the range of strains in a coating induced by a temperature gradient between the surface and the cross-sectional area of a sample wall increases. Such tests reveal the extreme manifestation of thermal stresses that is a thermal shock. They allow the comparison of coatings by their ability to realize deformation within the microzone of a coating. The typical feature of thermal shock testing is a formation of a network of small cracks in the coating. Their length does not exceed coating thickness. Cracks nucleate on cooling. At that period, the strains exceeding coating ductility arise in surface layers. The results of thermal shock tests carried out under 1050 °C ↔ cold water conditions are given in Table 7.19.

At such testing, an aluminized coating is fragmentized into a network of minor cracks after 8 to 10 cycles. The Ni20Cr12AlY coating is much more stable. It shows a network of cracks after 40 to 50 cycles. The addition of a highly ductile sublayer results in deceleration of crack growth and in changing the mechanism of their propagation from brittle to ductile. The advantages of the Ni20Cr12AlY coating tested under these conditions are due to a better ratio of TECs of an alloy and a coating and a respectively lower level of thermal stresses.

Thermal fatigue tests of coated samples have revealed that the coatings may both raise and reduce superalloy thermal fatigue. When carrying out short-term tests in air, which did not result in unprotected sample surface damage by oxidation, their lives could be longer than those of the samples with protective coatings.

The detrimental effect of coatings is caused by a wider range of strains on a coated alloy surface due to additional thermal stresses in the coating and lower mechanical properties of the coating in comparison with those of the superalloy. Similar to testing for creep-rupture strength, the situation changes at long-term testing or at testing in aggressive media, which prompt surface damage of unprotected samples.

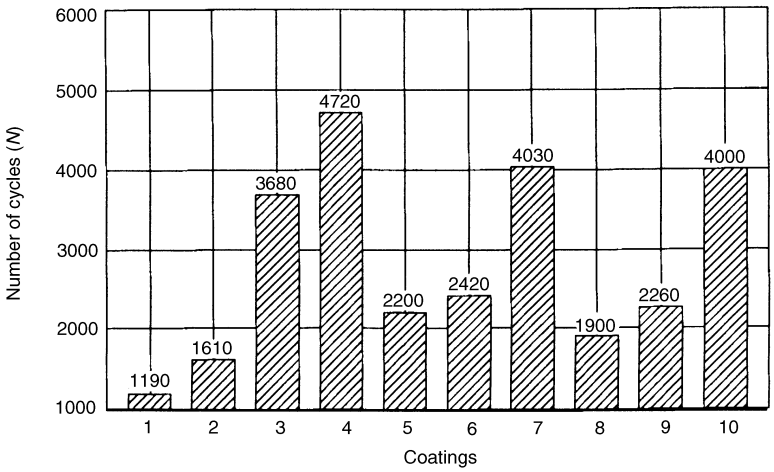

Fig. 7.31 Number of cycles to cracking caused by thermal fatigue of samples versus types of superalloys and coatings: JS6U superalloy (1, 2, 3, 4); JS30-SC superalloy (5, 6, 7); JS6F-DS superalloy (8, 9, 10). 1, 5, 8, Uncoated superalloy; 2, 6, 9, superalloy with aluminized coating; 3, superalloy with Ni20Cr12AlY coating; 4, 7, 10, superalloy with Ni20Cr12AlY/Ni10Co20Cr12AlY coating

Table 7.19 Thermal shock testing of different-type coatings. Test conditions: 1050 °C ↔ water

Alloy	Coating	Thickness, μm	Deposition method	Number of cycles before cracking of coating	Coating effect factor, $K = N/N_{Al}$
JS6F-DS	Aluminized	40	Aluminizing	8	…
JS6U-DS	Aluminized	40	Aluminizing	10	…
JS6F-SC	Aluminized	40	Aluminizing	10	…
JS6F-DS	Ni20Cr12AlY	100	EB	50 ÷ 60	5 ÷ 6
JS6F-DS	Ni20Co20Cr12AlY	100 m	EB	30 ÷ 40	3 ÷ 4
JS6F-DS	Ni20Cr12AlY/Ni10Co20Cr12AlY	40/60	EB	50 ÷ 70	5 ÷ 7

Distinctions in service lives of the samples with different coating compositions are caused by a number of factors, such as the level of thermal stresses arising in the coating, its ductility, and the strength and protective properties. The efficiency of any coating type manifests itself, to a greater extent, at high thermal stresses in a coating, which are generated by high rates of heating and cooling.

Coating Effect on Superalloy Low-Cycle Fatigue. Low-cycle fatigue tests are an efficient technique for evaluation of coating resistance to cracking caused by high strains typical of thermal loading. Flat samples 1 mm thick of the VJL12U superalloy with coatings of different compositions were tested for low-cycle fatigue by bending at 20 and 800 °C. At 20 °C, all types of coatings tested have ductility less than 1% and the maximum thermal stress level. At 800 °C, all coatings are ductile and thermal stresses are not high in them.

An aluminized coating deposited from a mixture of 98% Al-Fe alloy (36% Al) and 2% NH_4Cl and the Ni20Cr12AlY and Ni20Cr12AlY/Ni10Co20Cr12AlY overlay coatings 100 mm thick deposited by EB technique have been tested. The test results are presented in Fig. 7.32 and given in Table 7.20. At 20 °C, all types of protective coatings reduce life of the VJL12U superalloy. This feature is most conspicuous in the samples with the Ni20Cr12AlY coating and caused by defects (microdots) in them, which are stress concentrators. A two-layer coating affects their lives to a lesser extent. Unlike overlay coatings, diffusion coatings are under compressive stresses at 20 °C. However, despite it, they also shorten lives of the samples made of the VJL12U superalloy 5 to 7 times.

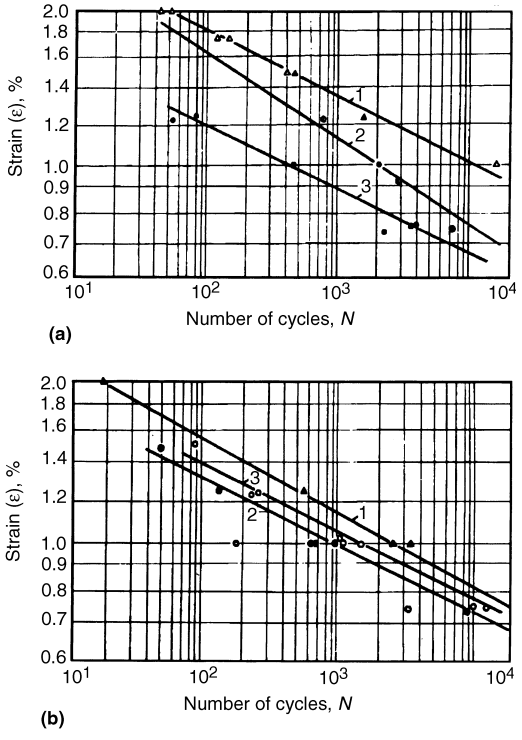

Fig. 7.32 Low-cycle fatigue of VJL12U superalloy at (a) 20 °C and at (b) 800 °C. 1, Uncoated; 2, aluminized coating; 3, Ni20Cr12AlY coating

During testing (<100 h) at 800 °C, no failure of the coating surface caused by oxidation occurs. Under these conditions, the coatings do not exhibit their protective properties, and accumulation of strains in them due to low yield strength enhances cracking and sample failure. Overlay coatings having high strength and ductility margin at 800 °C shorten sample lives to a lesser extent in comparison with diffusion coatings (Fig. 7.32). The lives of coated and uncoated samples differ less and less and have a tendency of becoming equal if cyclic testing lasts long enough. The relationships derived for the VJL12U superalloy can be extended to other superalloys.

It is worth determining coating material low-cycle fatigue separately from that of a superalloy and comparing these results with coated sample test results. A batch of samples was fabricated from the Ni20Cr12AlY alloy condensate produced by EB evaporation technique. The samples were 0.6 to 0.8 mm thick. Low-cycle fatigue testing was carried out by tension at 950 °C under two sets of test conditions:

- On testing under the first set of test conditions, certain loads were cyclically applied to the samples (4 cycles/min). Their levels neither varied nor depended on sample strains.
- On testing under the second set of test conditions, samples were cyclically strained. The strain range value, $\Delta\varepsilon$, did not vary at testing.

The test results are presented in Fig. 7.33(a) and (b) in comparison with the test results for the samples made of the JS26-DS superalloy, both uncoated and coated by the EA method with the Ni20Cr12AlY alloy 100 μm thick.

As a result of testing under the first and second sets of test conditions, lives of coated samples are longer than those of uncoated ones. This is due to the fact that coating ductility is very

high at 950 °C. A coating material sample tested under the first set of test conditions is shown in Fig. 7.34. Its ductility exceeds 100%. In both cases, the effect of the coating application is due to the JS26-DS superalloy surface protection against oxidation.

Under the first set of test conditions, when high mechanical properties are most conspicuous, the coated superalloy life is much longer than the coating material life. The conditions for loading a coating on a superalloy sample are fully dictated by the mechanical properties of a superalloy. Under these conditions, the coating accumulates failures much slower than a coating material tested separately does.

Under the second set of test conditions, in the certain range of strain range, a coating material has a longer life. This is also due to high ductility of the coating material at 950 °C. Failures in the superalloy that features lower ductility are accumulated much faster. Perhaps, coating failure occurs after cracking of the superalloy.

Coating Effect on Thermomechanical Fatigue of Superalloys

Basic Principles and Methods. The most detailed information on coating properties under conditions similar to blade service conditions can be obtained from thermomechanical fatigue (TMF) tests. For nickel-base superalloys used as turbine blade materials, the main TMF test types are load-adjusted thermomechanical fatigue test (LA-TMF test) and strain-control thermomechanical fatigue test (SC-TMF test) (Ref 25–27). At LA-TMF testing, a constant stress range of $\Delta\sigma = \text{const}$ (gentle loading) is preset, while at SC-TMF testing, a constant mechanical strain

Table 7.20 Experimental *K* and *C* in equation of $\Delta\varepsilon \cdot N^k = C$ characterizing low-cycle fatigue of VJL12U superalloy with coatings of different types

Test temperature	Coating	Thickness, μm	Deposition method	*K*	*C*
20 °C	Uncoated	…	…	0.119	3.11
	Aluminum	40	Aluminizing	0.215	4.99
	Ni20Cr12AlY	100	EB	0.127	2.15
	Ni20Cr12AlY/Ni10Co20Cr12AlY	100	EB	0.129	2.58
800 °C	Uncoated	…	…	0.144	2.97
	Aluminum	40	Aluminizing	0.126	2.34
	Ni20Cr12AlY	100	EB	0.131	2.56

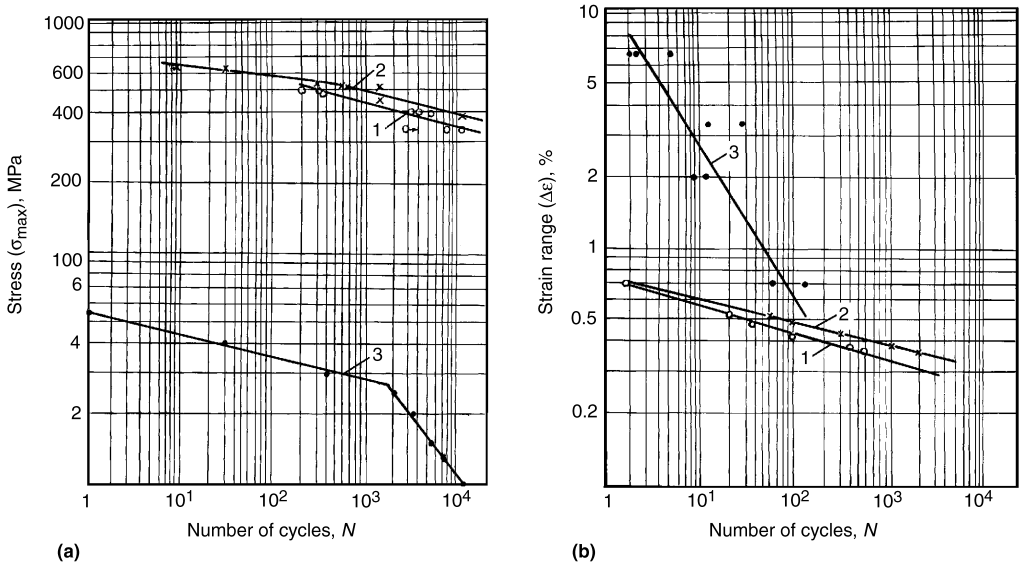

Fig. 7.33 Results of low-cycle fatigue testing of JS26-DS superalloy and vapor-deposited samples under (a) the first and (b) the second set of test conditions. 1, Uncoated superalloy; 2, superalloy with Ni20Cr12AlY coating; 3, samples made of condensate alloy Ni20Cr12AlY

range of $\Delta\varepsilon$ = const (severe loading) is usually held. At elastic deformation of a sample, both types of testing are, in fact, similar and thus yield similar outcome.

Each of the previously mentioned TMF tests allows only approximate simulation of blade-material deformation processes under service conditions, because in a real blade, complicated cyclic deformation takes place. This deformation is a combination of gentle loading caused by centrifugal and gas loads and of severe loading caused by thermal stresses. It is considered that severe cyclic loading that occurs at SC-TMF test is most similar to the real deformation conditions of a blade airfoil material. However, this statement is true under the conditions of elastic-plastic cyclic deformation of a blade material only when thermal stresses in a blade airfoil are noticeably higher than the mechanical stresses caused by centrifugal and gas loads. In addition, the irreversible creep strains take place in the blade airfoil under service conditions. This results in additional complication of a real blade material deformation pattern.

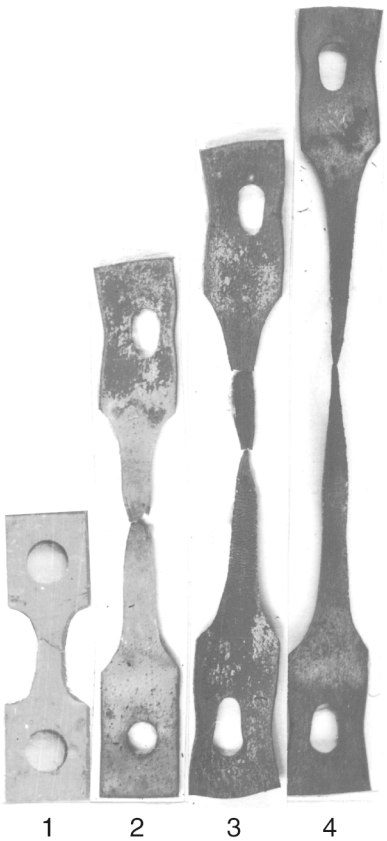

Fig. 7.34 Appearance of vapor-deposited Ni20Cr12AlY sample after testing under the first set of test conditions. 1, Initial sample; 2, σ = 55 MPa, δ = 320%; 3, σ = 25 MPa, δ = 240%, N = 2320 cycles; 4, σ = 15 MPa, δ = 500%, N = 5180 cycles

Both of the previously mentioned test methods are used for experimental investigations of TMF of overlay coatings deposited on turbine blades. In the case of experimental research into TMF of the coatings, the following factors typical of turbine blade coatings under their real deformation and failure conditions should be taken into consideration (Ref 28, 29):

- Basically, thermal fatigue cracking starts in the coating and then penetrates into the substrate. This is very typical for the SC blades cast with the primary crystallographic orientation ⟨001⟩ because of the low elasticity modulus of material and, therefore, low thermal strain ranges for thermal cyclic loading.
- It is necessary to take into account the two-axial stress state in the coating during analysis of the TMF test results of coated bars.
- Cracking of the coating on the cylindrical bar during TMF testing can be both diametrical and longitudinal.
- The stress-strain state of the coating cannot be directly measured by existing control methods during TMF testing of coated bars. For analysis of nonelastic straining of the coating under these conditions, it is necessary to use suitable constitutive models.
- Strains in coatings are basically dependent on the difference between TECs of the substrate and the coating. These strains in the coatings are usually non-linear (plastic) even when linear (elastic) straining of the substrate occurs. Coating strain range values are, as a rule, higher than corresponding strain range values of the surface layer of the blade (or bar) during thermomechanical cyclic loading, especially for the SC and DS materials.
- The number of cycles to the first crack initiation and their distribution on the outer surface of the SC blade airfoil cast with primary crystallographic orientation ⟨001⟩ depend on the secondary orientation of the crystallographic lattice in the airfoil cross section. This is greatly dependent on the circumferential thermal stresses, σ_s, in the blade, resulting in longitudinal coating cracking, and the value of circumferential elasticity modulus, E_s, for the SC superalloy. So, when TMF-cycle testing of SC-coated bar, it is necessary to know

the positioning of the axis of the secondary orientations of ⟨010⟩ and ⟨100⟩ for each bar, because distribution of the first crack on the coated surface can depend on this axis in the bar.

The following experimental method of TMF investigation of the protective coatings for turbine blades is suggested.

Because elastic-plastic straining of the coating is possible even under elastic straining of the substrate, it is suggested that TMF testing of the coated bars be carried out under conditions of elastic straining of the base material only. This method is expedient for SC turbine blades with primary crystallographic orientation ⟨001⟩, because there are no plastic strains in the outer layers of such blades at operating conditions. This is the result of the low elasticity modulus and high yield strength of blade material for the ⟨001⟩ orientation. The exceptions to the rule are small stress-concentration zones near perforation holes at the cooled blade walls where plastic strains of the blade metal are possible.

In accordance with that mentioned previously, the LA-TMF test is recommended for TMF testing of coated bars. The results of this method are similar to SC-TMF testing under conditions of elastic straining of the bar material but are simple in practice. The main problem for SC-TMF testing is the necessity for temperature uniformity of the metal in the extensometer-controlled zone at stationary and nonstationary thermal conditions. This is not necessary for the LA-TMF test, because during the test, the loading of the bar is controlled. Moreover, nonuniformity of temperature distribution along the central work zone with a temperature maximum is preferable, because it helps to fix the location of maximum failure in the cross section of the bar.

Using standard whole cylindrical bar with constant square cross-sectional work zone is recommended for the LA-TMF test. The stress state of the coating applied to the outer surface of the bar is biaxial, although the stress state of the bar itself during this test is uniaxial.

It is recommended to use a control system with two independent channels: first, to control the load, and second, to control the temperature of the bar during LA-TMF testing. This control system makes possible model changes in stress and maximum temperature of the work zone of the bar versus time with any phase shift among these independently controlled parameters. The possibility of stress asymmetry, $R_\sigma = \sigma_{min}/\sigma_{max}$, varying for all types of LA-TMF tests must also be limited. (σ_{min} and σ_{max} are correspondingly minimum and maximum values of stress during cycle.)

The stress-strain state of the bar coatings is calculated for the TMF test conditions by using the developed constitutive model based on the deformational theory of plasticity.

The calculational hysteresis loop for the overlay coating Ni20Co20Cr12AlY, obtained on the basis of this constitutive model for the out-of-phase LA-TMF test of the coated bar cast of MAR-M-002 superalloy, is shown in Fig. 7.35(a). The calculations are performed for out-

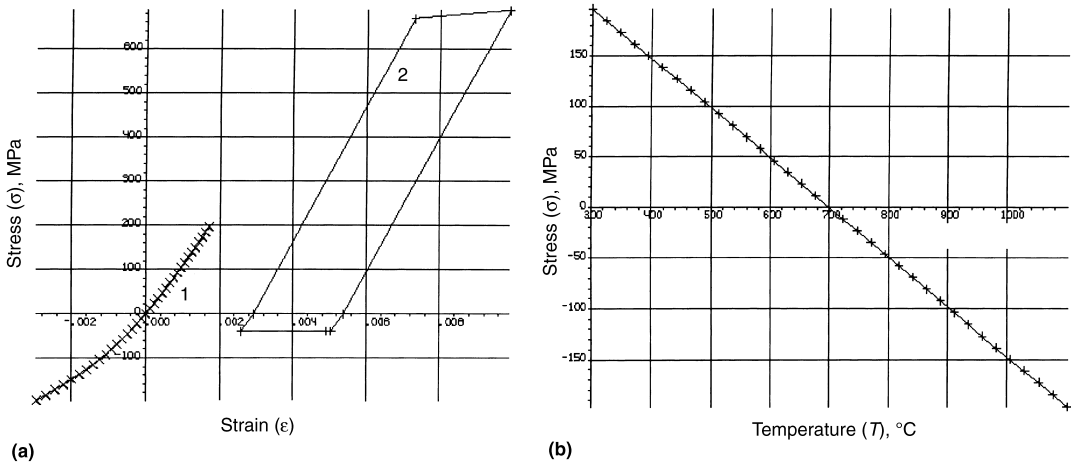

Fig. 7.35 Hysteresis loops for (1) MAR-M-002 bar and (2) Ni20Co20Cr12AlY coating material of (a) whole cylindrical coated bar and (b) when out-of-phase TMF testing

of-phase LA-TMF test conditions shown in Fig. 7.35(b) for a solid cylindrical specimen made of the MAR-M-002 superalloy with the Ni20Co20Cr12AlY coating.

For coating design, the mechanical properties of cast specimens of the same chemical composition as the coating material were used in a first approximation. It is worthwhile to perform the calculations in question before testing, because it allows the proper choice of test conditions for coated specimens capable of realizing the required range of elastic-plastic strains in the coating. It is also worthwhile to perform calculations based on real measurements of the sample temperature and the load applied after testing, for estimation of the actual strain range in the coating.

Calculations of strains in the coatings after testing are also required for plotting thermal fatigue curves specialized for coatings. For this purpose, sample thermal fatigue curves plotted from LA-TMF test data are used.

Thermomechanical Test Results for CMSX-4 Superalloy with Coatings. Three modifications of the coating were deposited on the test specimens (Ref 29, 30). The first modification of the coating ~80 μm thick was deposited by EA method. After its deposition, the coated specimens were annealed at 1080 °C for 2 h. Then, they were shot peened with microballs and underwent another annealing under vacuum at 1080 °C for 2 h. The coating features a dense, fine-grained structure typical of coatings deposited by EA method. The coating characteristics are presented in Table 7.21.

The second modification of the coating designated as Ni7Co12Cr17Al under study was deposited in two stages. At the first stage, a layer of the Ni8Co12Cr7Al coating was deposited by the previously mentioned technological process. At the second stage, a layer of Al-5%Si-1.5%Y alloy was deposited on the surface of Ni8Co12Cr7Al layer by EA method at the rate of 40 g/m^2. A diffusion layer ~50 μm thick was formed on the surface on annealing at 1080 °C for 2 h. The total coating thickness was ~80 μm. The average chemical compositions in the inner and outer zones of the coating are given in Table 7.21. The outer zone of the Ni7Co12Cr17Al coating consists of β-phase. Its structure is typical of the diffusion coatings deposited by EA method (Fig. 4.21d). A multiphase zone is formed under β-phase layer on diffusion annealing.

The Co32Ni21Cr8Al coating 100 to 120 μm thick was deposited by the low-pressure plasma spray (LPPS) method using the same technological process as for turbine blades.

Thermomechanical Fatigue Tests. Proceeding from the principles discussed previously, the following test conditions were used: temperature and load antiphase alteration, and asymmetric cycle of load alteration without holding the specimen at the maximum cycle temperature (Fig. 7.36).

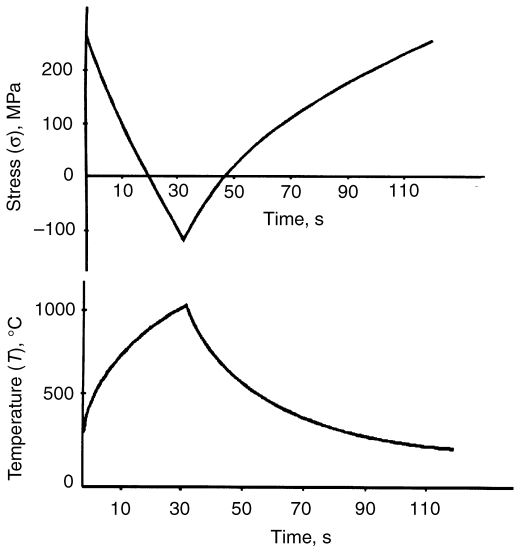

Fig. 7.36 Stress and maximum temperature vs. time distribution during out-of-phase LA-TMF testing of coated bar

Table 7.21 Characteristics of coatings tested

Coating	Deposition method	Thickness, μm	Coating zone	Chemical composition, wt%						
				Ni	Co	Cr	Al	Ta	Re	Hf
Ni8Co12Cr7Al	EA	80	…	Base	7.6	12.4	6.5	4.5	0.3	0.4
Ni7Co12Cr17Al	EA	80	Outer	Base	6.5	7.5	17.0	2.0	0.2	…
	EA	…	Inner	Base	8.1	16.9	6.8	4.5	1.1	0.5
Co32Ni21Cr8AlY	LPPS	100–120	…	32	Base	21	8	…	…	…

Note: EA, electric arc; LPPS, low-pressure plasma spray

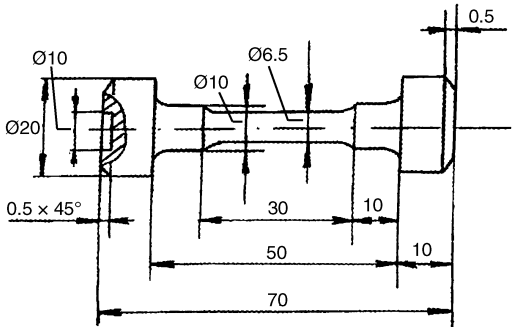

Fig. 7.37 Specimen for TMF tests (in mm)

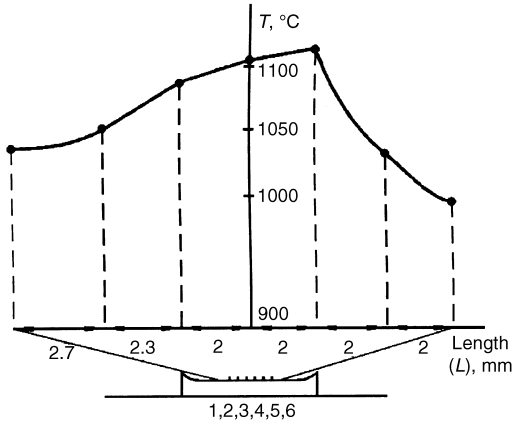

Fig. 7.38 Temperature pattern in specimen working area

Table 7.22 Specimen loading conditions

No.	Temperature, °C	Stress, MPa	Stress range, MPa
1	100	$\sigma_{tensile} = +500$	$\Delta\sigma = 650$
	1100	$\sigma_{compressive} = -150$	
2	100	$\sigma_{tensile} = +200$	$\Delta\sigma = 350$
	1100	$\sigma_{compressive} = -150$	
3	100	$\sigma_{tensile} = +200$	$\Delta\sigma = 300$
	1100	$\sigma_{compressive} = -100$	
4	100	$\sigma_{tensile} = +200$	$\Delta\sigma = 250$
	1100	$\sigma_{compressive} = -50$	

Whole cylindrical specimens of the CMSX-4 superalloy with diameters of 6.5 mm were used to carry out TMF tests (Fig. 7.37). Specimens were heated by conducting electric current with current density of $I = 20$ A/mm^2. The temperature distribution pattern in the specimen working zone is given in Fig. 7.38. Earlier research has revealed that the previously mentioned heating conditions do not cause changes in superalloy mechanical properties (Ref 31). At the same time, specimens were loaded using a hydraulic loading device. The main parameters of specimen loading conditions are presented in Table 7.22.

The coating service life was set by the moment when cracking on the surface was detected. Control over cracking was carried out by an optical method and by nondestructive liquid-penetrant testing. The resolving power of the technique in use was as follows: crack length ≥0.5 mm and depths of penetration of ~0.05 mm.

To specify specimen-loading conditions during the testing cycle, strain was measured in the zone of the maximum temperature. Marks made of the wire with a diameter of 0.05 mm were spot welded to the specimen surface. The distance between the marks was measured at the minimum and maximum temperatures of the cycle using an optical measuring device (Fig. 7.39). Then, measurements were carried out at heating under mechanical loading, and the total strain was calculated in the central zone of the specimen. The total strain range versus the applied stress range in the center of the specimen is shown in Fig. 7.40.

For each coating modification, fatigue tests under thermal cycling were carried out at three levels of stress amplitudes in the specimen. Based on the experimental data, a thermomechanical fatigue curve was plotted on the stress

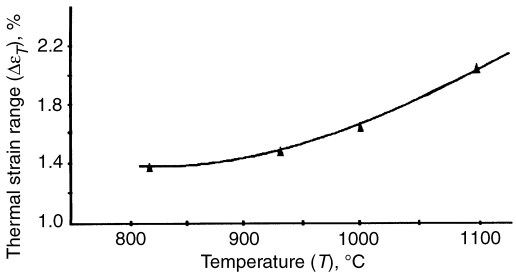

Fig. 7.39 Thermal strain range distribution in the specimen maximum temperature area

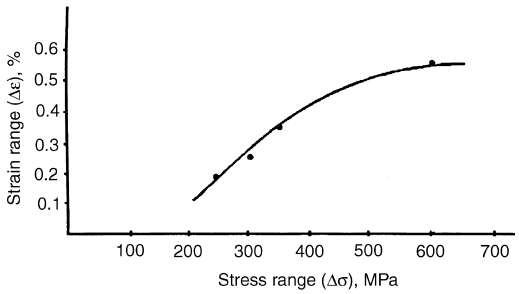

Fig. 7.40 Strain range, Δε, of specimen versus stress range, Δσ, in the maximum temperature area

range ($\Delta\sigma$, MPa)-service life (N, cycles) coordinates.

The terms used for test data description are as follows: coating service life is the number of cycles to crack(s) detection on the coated specimen surface, and CMSX-4 superalloy service life is the number of cycles to crack(s) detection on the uncoated specimen surface.

Service lives of uncoated specimens of the CMSX-4 superalloy tested by the previously mentioned method are of much interest, because these data may be used for comparison with coating service lives and the analysis of the effect of coatings on the alloy properties. When cracking was detected on the specimen surface, the test was not terminated. It was run to failure of the specimen. Test results are given in Table 7.23 and Fig. 7.41.

Fractographic study of the specimens has shown that they are typical of the failure at TMF testing at narrow stress range. The nucleation site of the crack is situated on the specimen surface (Fig. 7.42). The cracks grow into the specimen and cause its failure. During testing, most of the cycles are spent on crack nucleation on the specimen surface. After crack nucleation, the service life of the cracked specimen is up to 8 to 20% of the total service life of the specimen under study. Measuring specimen dimensions after their testing has revealed no elongation or changes of their diameters. This is evidence of the compliance of the tests with the chosen loading conditions in the range of superalloy elastic deformation.

Table 7.23 Uncoated CMSX-4 alloy specimen test results

Number of cycles to cracking	Number of cycles to specimen failure	Stress range ($\Delta\sigma$), MPa
2850	3630	650
6190	6510	650
…	4840	650
15,780	16,950	450
20,420	21,820	350
48,670	…	300
24,120	25,480	300
41,270	44,860	250

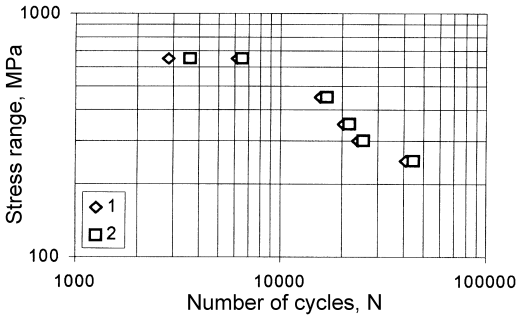

Fig. 7.41 Cyclic life of CMSX-4 superalloy. 1, Cracks on surface specimen; 2, failure of specimen

Test results for the specimens with the Co32Ni21Cr8AlY coating are shown in Fig. 7.43. The number of cycles to crack appearance on the specimen surface with the Co32Ni21Cr8AlY coating is much less than for an uncoated specimen. Crack appearance and spacing in the surface network are similar to those typical of thermal fatigue cracks, which develop in the coatings on blade surfaces (Fig. 7.44). The cracks were detected along the full length of the specimen. There were cracks in the areas where the maximum temperatures did not go over 1000 °C. Crack nucleation is a consequence of the accumulation of plastic strain in the coating as well as the formation of pores and minor surface ruptures, which join together gradually and form a thermomechanical fatigue crack in the coating (Fig. 7.45a,b).

Crack propagation rate in the CMSX-4 superalloy is much less than that in the coating. While cracks ~80 to 100 μm long were detected in the coating after 1000 cycles, a further 3100 cycles resulted in crack penetration of not more than 100 to 120 μm into the alloy. Test results for specimens with the Ni8Co12Cr7Al coating are shown in Fig. 7.43.

The mechanism of crack formation and their appearance and surface network are identical with those typical of specimens with the Co32Ni21Cr8AlY coating. The Ni8Co12Cr7Al coating service life is 4 times as long as that of the Co32Ni21Cr8AlY coating at the stress range of $\Delta\sigma = 300$ MPa and 2 times as long at the stress range of $\Delta\sigma = 250$ MPa.

Test results for specimens with the Ni7Co8Cr17Al coating are shown in Fig. 7.43. The mechanism of crack formation and their appearance and surface network are identical with those typical of specimens with the Co32Ni21Cr8AlY and Ni8Co12Cr7Al coatings. The Ni7Co12Cr17Al coating service life is 13 times as long as that of the Co32Ni21Cr8AlY coating at the stress range of $\Delta\sigma = 300$ MPa and 8 times as long at the stress range of $\Delta\sigma = 250$ MPa.

Mechanism of Coating Effect on Thermomechanical Fatigue of Superalloys. A coating with physical and mechanical properties identical to those of the protected superalloy can be

considered as an "ideal" coating, with high thermomechanical fatigue resistance. This coating can hardly be developed, because a thin layer of polycrystalline coating cannot have mechanical properties typical of a modern SC superalloy. However, the development of a coating with characteristics that are as similar to those of the uncoated superalloy as possible is an advantageous line in producing a coating with high thermal fatigue resistance.

The use of LA-TMF test methods with anti-phase change in temperatures and stresses allows the simulation of stress and strain conditions in the coatings on turbine blade surfaces. Under the selected test conditions, the applied loads contribute to the increase in compressive stresses in coatings at high temperatures and to the increase in their tensile stresses at low temperatures. The test technique in use allows the distinctions in coating resistance to thermal fatigue crack nucleation and propagation to be revealed.

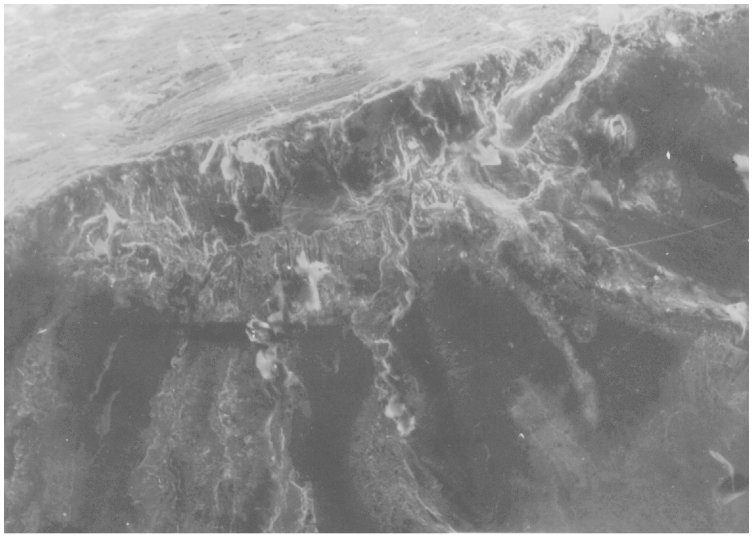

(a)

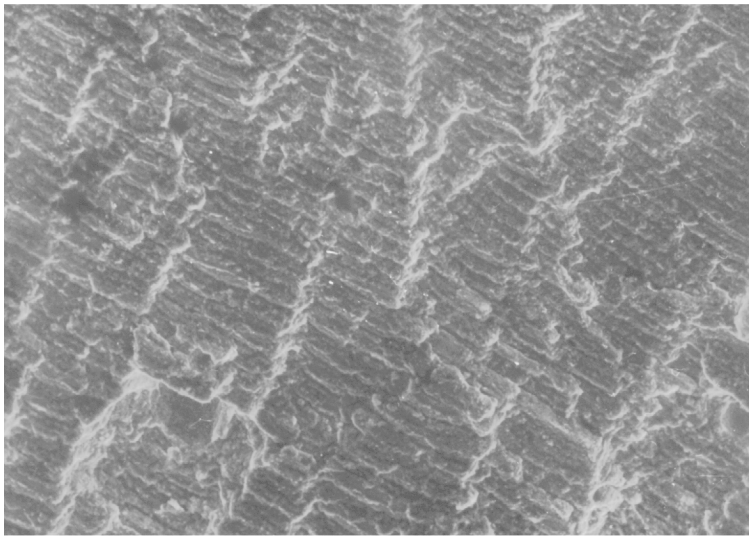

(b)

Fig. 7.42 Fracture of specimen CMSX-4 superalloy, 3658 cycles, $\Delta\sigma = 650$ MPa. (a) Site of failure, 200×; (b) crack development area, 500×

Table 7.24 Comparison of average lives of uncoated CMSX-4 specimens and CMSX-4 specimens with different coatings

Stress range (Δσ), MPa	Number of cycles to cracking (%)			
	CMSX-4	Co32Ni21Cr8AlY	Ni8Co12Cr7Al	Ni7Co12Cr17Al
650	2850 (100%)	368 (13%)	…	…
350	20420 (100%)	…	2840 (14%)	10550 (52%)
300	24120 (100%)	911 (4%)	4178 (17%)	12484 (52%)
250	41270 (100%)	2330 (6%)	6592 (16%)	18587 (45%)

Specimen fractography after thermal fatigue testing has revealed that, in all cases, the crack nucleation sites are located on the specimen surfaces and the fracture type is similar to that caused by applying alternating loads. Cracks are developed in the coatings after accumulation of considerable strain. The tests have revealed a noticeable distinction between the time to thermomechanical fatigue crack detection on the uncoated specimens and on the specimens with different coatings.

All test data are given in Table 7.24 for comparison. The Co32Ni21Cr8AlY coating service life is only 6 to 8% of uncoated CMSX-4 alloy service life. Thus, if there are zones in turbine blades with the stress range similar to that used at testing, numerous thermal fatigue cracks will develop in the Co32Ni21Cr8AlY coatings on their surfaces. The development of these cracks on the blades may be unexpected, because, as a rule, coating service life is not taken into account in blade service-life calculations.

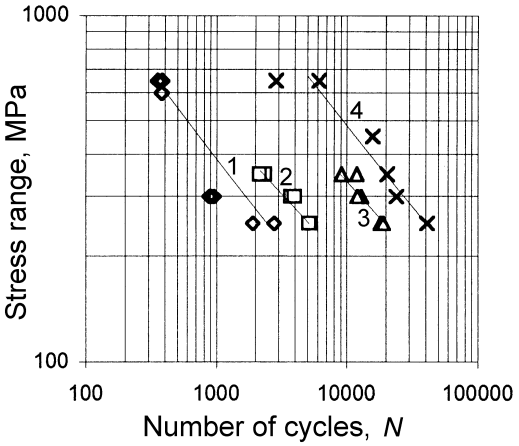

Fig. 7.43 Cyclic life of uncoated CMSX-4 superalloy (4) and CMSX-4 with coatings. 1, Co32Ni21Cr8AlY coating; 2, Ni8Co12Cr7Al coating; 3, Ni7Co12Cr17Al coating

Fig. 7.44 Crack location on specimen surface with Co32Ni21Cr8AlY coating (liquid penetrant testing), 900 cycles

Changes in coating physical-chemical properties can have a significant effect on their service lives. The Ni8Co12Cr7Al coating service life is 2 to 4 times as long as that of Co32Ni21Cr8AlY coating. The Ni7Co12Cr17Al coating has also demonstrated high service life. The Ni7Co12Cr17Al coating service life is 8 to 10 times as long as that of the Co32Ni21Cr8AlY coating, and it is 45 to 52% of the CMSX-4 superalloy service life. This service life is primarily due to close agreement of linear TECs of the coating and the CMSX-4 superalloy. However, the effect of technological factors in forming the outer diffusion layer from a melted aluminum-base liquid phase cannot be excluded. The presence of the outer diffusion layer has a desirable effect on the coating service life, too. As is known, unlike the applied coatings, diffusion coatings accumulate residual compressive stresses in the temperature range below 900 °C.

The chosen testing technique that uses the specimens with diameters of 7 mm does not allow the estimation of the effect of crack formation in the coating on CMSX-4 specimen service lives. The comparison of the number of cycles to failure for coated and uncoated specimens has revealed that the number of specimens tested to failure and the test data are insufficient for unbiased estimation of this effect.

The agreement of the test data from the coating service lives on the specimens with those on the blades depends on blade service conditions in the engine. In short-term cyclic tests of the engines under high thermal loading conditions,

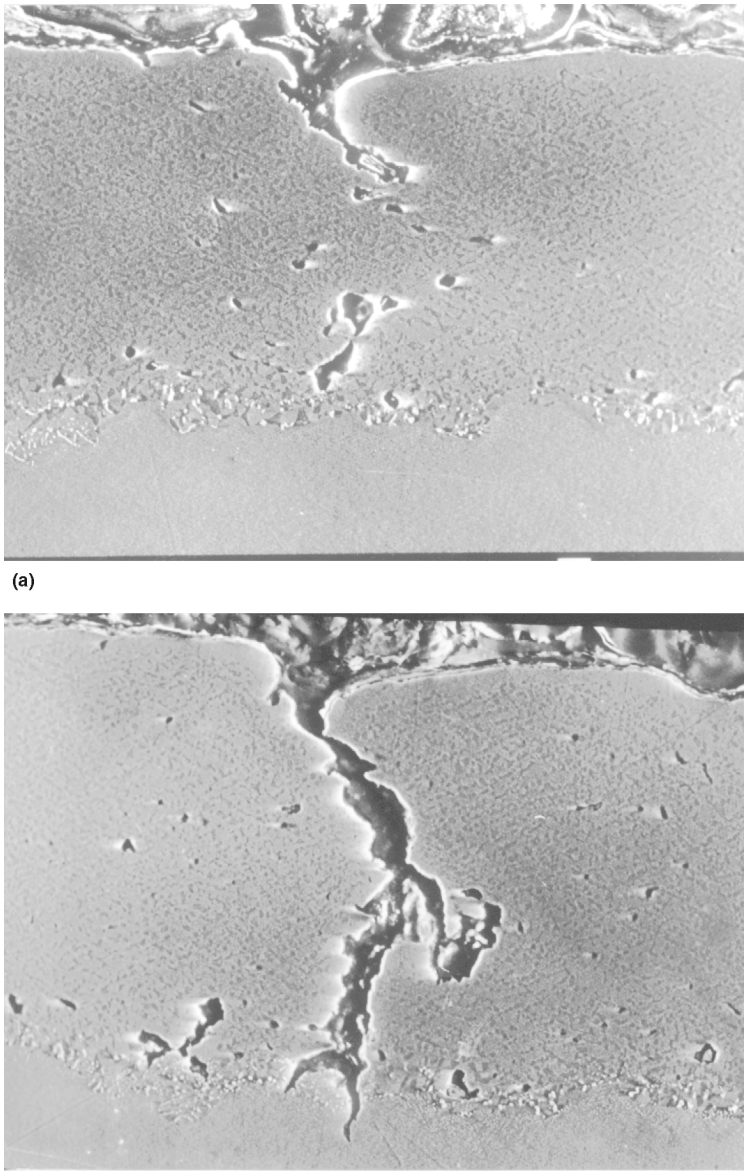

Fig. 7.45 Cracks in Co32Ni21Cr8AlY coating at (a) the initial stage of crack development and (b) the stage of its propagation into the superalloy after 550 cycles. 500×

there is a high probability that the data from the coating service lives on the blades will show close agreement with the respective results of laboratory testing of the specimens. In the case of long-term tests in the engines, these data will depend to a considerable extent on such coating characteristics as oxidation resistance and resistance to hot corrosion.

REFERENCES

1. M.I. Wood, The Mechanical Properties of Coatings and Coated Systems, *High Temperature Corrosion Advanced Materials and Coatings,* R. Streiff, J. Stringer, R. Krutenat, and M. Caillet, Ed., Elsevier Science Publishers, 1989, p 633–643

2. P.T. Kolomytzev, *Gas Corrosion and Strength of Nickel Alloys*, Moscow, Metallurgy, 1984, 216 p
3. E.M. Grale, Research into NiAl and Ni_3Al, *Mechanical Properties of Intermetallic Compounds,* J.H. Westbrook, Ed., John Wiley & Sons, New York, 1960, p 266–299
4. A.G. Rozner and R.J. Wasilelevski, Tensile Properties of NiAl and Ni_3Al, *J. Inst. Met.,* Vol 94 (No. 5), 1966, p 169–175
5. V.P. Buntushkin and O.A. Bazyleva, Casting Ni_3Al Intermetallic Compound-Base Alloy for Single-Crystal Engine Turbine Rotor Blades, *Aviatsionnaya Prom-st.,* N 3–4, 1997, p 61–65
6. G.W. Goward, Current Research on the Surface Protection of Superalloys for Gas Turbine Engines, *J. Met.,* Vol 22 (No. 10), 1970, p 31–39
7. P.T. Kolomytzev and N.V. Abraimov, Research into Temperature Effect on Coatings Ductility, *Phys. Chem. Mech. Mater.,* No. 2, 1982, p 104–107
8. Y.S. Eliseev, N.V. Abraimov, and V.V. Krymov, *Chemical-Heat Treatment and Protective Coatings in Aircraft Engine-Building,* Moscow, Vysshaya Shkola, 1999, 525 p
9. V.I. Nikitin, Y.A. Tamarin, and N.V. Zabrodina, Investigations of Structural and Physical-Chemical Characteristics of Ni-CoCrAl System Alloys, *Protective Coating Application and Use,* Leningrad, Nauka, 1987
10. A.I. Krivko, A.I. Epishin, and A.I. Samoilov, X-Ray Method of Research into Stressed-Strained State of Composite Materials Based on Calculations and Experiments, *Zavod. Lab.,* Vol 1 (No. 5), 1985, p 34–38
11. A.I. Samoilov, I.A. Ignatova, A.M. Vorobiev, and V.S. Kozlova, Measurements of Thermal Stresses in Ni-(Co)-Cr-Al-Y Heat-Resistant Coatings, *Zavod. Lab.,* Vol 50 (No. 11), 1984, p 36–39
12. E.G. Kuzovkov, *Numerical Simulation of Stressed State for Strained Bodies by Elementary Cells Method,* Kiev, Institute of Strength Problems, 1981, 37 p
13. V.I. Nikitin, *Corrosion and Protection of Gas Turbine Blades,* Leningrad, Machinostroenie, 1987, 272 p
14. V.I. Nikitin and I.P. Komossarova, Method of Protective Coating Testing for Lifetime, *Proc. CKTI,* (No. 176), 1980, p 67–73
15. V.I. Nikitin, Y.A. Tamarin, and N.V. Zabrodina, Corrosive and Mechanical Properties of Protective Coatings, *Aqueous-Chemical Conditions and Corrosion of Power Equipment,* No. 201, Leningrad, CKTI, 1986, p 72–81
16. J.F. Paskiet, D.H. Boon, and C.P. Sullivan, Effect of Aluminide Coating on High-Cycle Fatigue Behavior of Nickel-Base High-Temperature Alloy, *J. Inst. Met.,* Vol 100 (No. 2), 1971, p 58–62
17. M.M. Gell, G.P. Leverant, and C.H. Wells, The Fatigue Strength of Nickel-Base Superalloys, *ASTM STR,* No. 64, 1970, p 113–153
18. I.I. Ischenko, V.I. Omelchenko, and B.N. Sinaisky, Research into Effect of Heat-Resistant Coatings on Superalloy Fatigue Strength, *Strength Probl.,* No. 10, 1971, p 76–79
19. I.I. Ischenko, V.I. Omelchenko, and B.N. Sinaisky, Research into Effect of Heat Treatment and Protective Coatings on JS6K Superalloy Fatigue Strength, *Strength Probl.,* No. 8, 1976, p 10–15
20. L.M. Akimov, *Superalloys Fatigue Lives,* Moscow, Metallurgy, 1977, 220 p
21. P.T. Kolomytzev and P.G. Lebedev, Cyclic and Long-Term Rupture Strength of Alloys with Protective Coating, *Strength Probl.,* No. 9, 1972, p 92–95
22. L.B. Getsov, A.I. Rybnikov, and I.S. Malashenko, Fatigue Resistance of Coated Superalloys, *Strength Probl.,* No. 5, 1990, p 51–56
23. T.N. Rhys-Jones and T.P. Cunningham, The Influence of Surface Coatings on the Fatigue Behaviour of Aero Engine Materials Surface and Coatings Technology, Vol 42, 1990, p 13–19
24. L.P. Lozinsky, B.I. Musienko, and A.A. Ivanenko, Effect of Diffision Coatings on Turbine Blade Damage at Thermal Cycling, Vol 8, Kiev, Naukova Dumka, 1974, p 134–136
25. G.R. Halford, T.G. Meyer, R.S. Nelson, and D.M. Nissley, "Fatigue Life Prediction Modeling for Turbine Hot Section Materials," NASA Technical Memorandum 100291, 33rd Intl. Gas Turbine and Aeroengine Congress and Exposition, (Amsterdam, The Netherlands), ASME, 5–9 June 1988
26. E.G. Ellison, Thermomechanical Strain Cycling and Testing at Higher Temperature,

Measurement of High Temperature Mechanical Properties of Materials, M.S. Loveday and M.F. Day, Ed., HMSO, London, 1982, p 204–218

27. D.A. Miller and R.H. Priest, Materials Response to Thermal Mechanical Strain Cycling, *High Temperature Fatigue: Properties and Prediction,* R.P. Skelton, Ed., Elsevier Applied Science, 1987, p 113–175
28. Y.A. Nozhnitsky, R.A. Doulnev, and V.G. Sundyrin, Damage Mechanisms for Thermomechanical Fatigue of Aircraft Engines Materials, 81st Meeting of the AGARD SMP, (Banff, Canada), 2–4 Oct 1995, and published in *CP-559*
29. Y.A. Tamarin, V.G. Soundyrin, and N.G. Bychkov, Thermo-Mechanical Fatigue Tests of Coatings for Turbine Blades, *High Temperature Surface Engineering,* J. Nicholls and D. Rickerby, Ed., IOM Communications Ltd., 2000, p 157–169
30. Y.A. Tamarin and H.C. Low, Thermal Fatigue of Protective Coatings on CMSX-4 Superalloy, *High Temperature Corrosion 5,* R. Streiff, I.J. Wright, R. Krutenat, M. Caillet, and A. Cailerie, Ed., Trans Tech Publication, 2001, p 647–654
31. N.G. Bichkov, Test Rig for Thermo-Mechanical Fatigue Tests, *Zavod. Lab.,* Vol 57 (No. 12), 1991, p 57–58.

Protective Coatings for Turbine Blades
Y. Tamarin, p161-193
DOI: 10.1361/pctb2002p161

CHAPTER 8

Electron Beam Thermal Barrier Coatings

DEVELOPMENT of thermal barrier coatings (TBCs) applied to cooled blades is one of the trends for improving gas turbines. Unlike aluminide protective coatings, ceramic coatings not only protect blade surfaces from high-temperature oxidation and corrosion but also prevent base material softening at high temperatures. Thermal barrier coating application allows the reduction of the blade temperature and the significant increase in its service life. Under both steady-state and transient conditions, the application of TBCs can diminish temperature gradients over the blade surfaces as well as reduce thermal stresses in them.

Between 1980 and 2000, a great number of scientific papers and patents were published. They covered the issues concerning development, deposition techniques, and use of TBCs. A typical design of a TBC is presented in Fig. 8.1. The ceramic layer deposited directly on the superalloy surface does not show the required service life. Penetration of oxygen through the ceramic layer to the superalloy surface results in its quick oxidation and in spallation of the ceramic layer. That is why, as a rule, a TBC consists of at least two layers. An inner aluminide heat-resistant bond coat may be formed by different techniques. It may be either a diffusion or an overlay coating, depending on the requirements of its physical-mechanical properties and protection targets. The requirements of bond coat properties and protective coatings properties are much the same, yet the bond coat should meet some special requirements. First of all, it must be highly heat resistant; the oxides formed on its surface should have high adhesion to both the bond coat and the outer ceramic layer. When choosing a bond coat composition, one should pay special attention to its yttrium content as well as to the contents of the other elements, which guarantee high oxide adhesion to the surface and reactive element effect (Ref 1). It is of special importance for bond coats deposited by the electron beam (EB) technique, because their yttrium contents depend on the yttrium content of the liquid bath and vary within wide limits (Ref 2). In this case, the required yttrium content of 0.2 to 0.3% is guaranteed by different technological procedures, such as direct yttrium addition to the liquid bath. Under these conditions, it is noteworthy that high yttrium contents of the liquid bath cause slag formation on its surface, thus resulting in occurrence of microdrops. These microdrops on the bond coat surface may provoke defects in the ceramic layer.

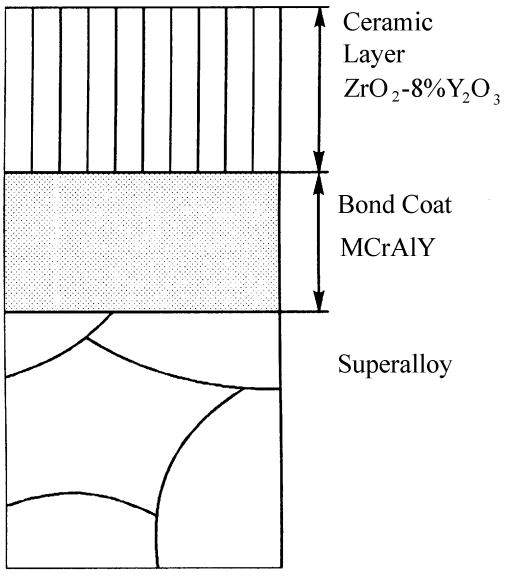

Fig. 8.1 Thermal barrier coating design